Published in final edited form as:
Hum Genet. 2014 May ; 133(5): 599–616. doi:10.1007/s00439-013-1391-3.

COOH-Terminal Collagen Q (*COLQ*) Mutants Causing Human Deficiency of Endplate Acetylcholinesterase Impair the Interaction of ColQ with Proteins of the Basal Lamina

Juan Arredondo, **Marian Lara**, **Fiona Ng**, **Danielle A. Gochez**, **Diana C. Lee**, **Stephanie P. Logia**, **Joanna Nguyen**, and **Ricardo A. Maselli**[1]
Department of Neurology, University of California Davis, Davis, CA 95618

Abstract

Collagen Q (ColQ) is a key multidomain functional protein of the neuromuscular junction (NMJ), crucial for anchoring acetylcholinesterase (AChE) to the basal lamina (BL) and accumulating AChE at the NMJ. The attachment of AChE to the BL is primarily accomplished by the binding of the ColQ collagen domain to the heparan sulfate proteoglycan perlecan and the COOH-terminus to the muscle-specific receptor tyrosine kinase (MuSK), which in turn plays a fundamental role in the development and maintenance of the NMJ. Yet, the precise mechanism by which ColQ anchors AChE at the NMJ remains unknown. We identified five novel mutations at the COOH-terminus of ColQ in seven patients from five families affected with endplate (EP) AChE deficiency. We found that the mutations do not affect the assembly of ColQ with AChE to form asymmetric forms of AChE or impair the interaction of ColQ with perlecan. By contrast, all mutations impair in varied degree the interaction of ColQ to MuSK as well as basement membrane extract (BME) that have no detectable MuSK. Our data confirm that the interaction of ColQ to perlecan and MuSK is crucial for anchoring AChE to the NMJ. In addition, the identified COOH-terminal mutants not only reduce the interaction of ColQ with MuSK, but also diminish the interaction of ColQ with BME. These findings suggest that the impaired attachment of COOH-terminal mutants causing EP AChE deficiency is in part independent of MuSK, and that the COOH-terminus of ColQ may interact with other proteins at the BL.

Keywords

ColQ mutations; AChE activity; neuromuscular junction; congenital myasthenia syndromes; perlecan

INTRODUCTION

The enzyme acetylcholinesterase (AChE) plays a critical role at the neuromuscular synapse. AChE has serine hydrolase activity, which degrades acetylcholine (ACh) released from the presynaptic nerve endings into choline and acetate (Katz and Miledi 1965; Rosenberry 1979). Once ACh is unbound from the acetylcholine receptor (AChR), the rapid catalytic

[1]To whom correspondence should be addressed: Ricardo A. Maselli, Department of Neurology, University of California Davis, 1515 Newton Court, Room 510, Davis, CA 95618, USA, Tel: +1 5307545019; Fax: +1 5307545036; ramaselli@ucdavis.edu.

activity of AChE blocks subsequent binding of ACh to the receptor, and consequently limits the duration of the synaptic activation (Katz and Miledi 1973).

The AChE collagenic tail peptide (ColQ) is a non-fibrillar collagen subunit, which assembles through its NH_2-terminal proline-rich attachment domain (PRAD) to the tryptophan amphiphilic tetramerization (WAT) sequence (Dvir et al. 2004), located at the COOH-terminus of the major splice variant (T) of the AChE ($AChE_T$) subunit (Legay et al. 1995; Massoulié et al. 1998; Simon et al. 1998). ColQ has two additional domains (Fig. 1a): a collagenic domain that interacts with perlecan through two heparan sulfate proteoglycan (HSPG) motifs (Deprez and Inestrosa 1995; Deprez et al. 2003), and a COOH-terminal domain that interacts with the muscle-specific kinase (MuSK) (Cartaud et al. 2004; Nakata et al. 2013), and anchors the $AChE_T$ to the basal lamina (BL). ColQ is arranged in a triple helix that enhances its interaction with heparin (Deprez et al. 2000) while the NH_2-terminal PRAD of each of the helices interacts with the COOH-terminal domain of $AChE_T$ homotetramers, leading to the formation of various globular (Bon et al. 1997) and asymmetric forms of the enzyme (Bon et al. 2003; Younkin et al. 1982). ColQ and other collagens are known to organize their triple-helical structure in the endoplasmic reticulum. The structural characteristics of ColQ enable ColQ to function, like other collagens, as multidomain proteins (Brodsky and Shah, 1995; Prockop and Kivirikko, 1995). The trimerization of ColQ is initiated by the non-collagenous trimerization domain from its COOH-terminal region (Engel et al. 1991; McLaughlin and Bulleid 1998). The C-terminal trimerization domain (CTD) in human ColQ comprises residues 294–372, and a ten-cysteine-rich domain encompassing residues 375–451 (Krejci et al. 1991).

The mammalian skeletal muscle AChE displays rich molecular polymorphism (Legay 2000; Massoulié et al. 1999), because different enzyme isoforms driven by different promoters are expressed by alternative mRNA splicing (Legay et al. 1995; Li et al. 1991, 1993; Sikorav et al. 1988). Globular (G) molecular forms consist of one (G_1), two (G_2), or four (G_4) identical $AChE_T$ catalytic subunits. Heteromeric asymmetric forms are composed of one (A_4), two (A_8), or three (A_{12}) homotetramers attached to a structural subunit made of three ColQ strands (Massoulie et al. 1993; Rotundo and Fambrough 1994). Thus, depending on the number of catalytic $AChE_T$ subunits per collagen tail, there are A_4, A_8, and A_{12} molecular forms, where the A_{12} form is the most abundant enzyme complex found at the neuromuscular junction (NMJ) (Hall 1973; Krejci et al. 1991).

The enzyme asymmetric forms are absent at the NMJ in ColQ knockout mice lacking the PRAD domain, where unexpectedly the non-amphiphilic globular $AChE_T$ tetramers, G_4^{na}, are also missing in neonatal mice (Feng et al. 1999).

Human mutations in the ColQ gene (*COLQ*) result in deficiency of endplate (EP) AChE, which is a severe and recessively transmitted form of congenital myasthenia syndrome (CMS) (Engel et al. 2003). Most mutations in the NH_2-terminus and collagen domains of ColQ are truncation mutations that preclude the formation of A_{12} (Ishigaki et al. 2003; Ohno et al. 1998). In contrast, the majority of mutations occurring at the COOH-terminal domain of ColQ are missense mutations, which do not hinder the formation of A_{12} but interfere with the anchoring of the ColQ-$AChE_T$ complex to the BL (Ohno et al. 2000; Nakata et al. 2013).

Expression studies designed to assess the effect of *COLQ* mutations involve the co-expression of ColQ and $AChE_T$ in heterologous cells, followed by sucrose density gradient and Ellman assay analysis. Mutations in PRAD prevent assembly of $AChE_T$ with ColQ into the asymmetric A_4, A_8, and A_{12} forms of the enzyme, and the analysis shows only the globular peaks G1 and G2. Mutations in the collagen domain result in a single ColQ strand assembled with only one $AChE_T$ tetramer and generate a mutant peak (M). Finally, most COOH-terminal mutations do not alter the gradient profile and require complex biological assays, such as transplantation of purified AChE mutants into heterologous frog NMJ to assess their ability to interact with the BL of the NMJ (Kimbell et al. 2004). For this study, we have used a modification of the binding assay developed by (Vigny et al. 1983; Peng et al. 1999), based on the attachment of ColQ to plates coated with basement membrane extract (BME).

We are reporting here five novel missense mutations in the COOH-terminal domain of ColQ identified in seven patients from five independent families with AChE deficiency. As expected, the mutants did not prevent the assembly of ColQ with $AChE_T$ to form the heteromeric asymmetric forms or impede the interaction of ColQ with perlecan. However, all mutants varied in the degree to which ColQ interacted with MuSK and also impaired the binding of ColQ to BME extract lacking detectable MuSK. Our findings suggest that in addition to the interaction of ColQ with perlecan and MuSK, there are other important interactions of ColQ with other proteins of the BL that stabilize the attachment of AChE to the NMJ. These additional protein interactions are disrupted by COOH-terminal *COLQ* mutations causing CMS.

EXPERIMENTAL PROCEDURES

Cells and Reagents

Human embryonic kidney 293 (HEK-293) cells were kindly provided by Dr. Tsung-Yu Chen (University of California, Davis). Cultures were grown in DMEM supplemented with 10% FBS, L-glutamine, and penicillin/streptomycin mix, and incubated at 37°C/5% CO_2. HEK-293-EBNA cells were a generous gift from Dr. Cindy Farach-Carson (Rice University). These special HEK-EBNA cells, which are used for inducible expression of perlecan domain I (PlnDI), contain a unique segment of 172 residues to express a 22-kDa protein core that contains three Ser-Asp-Gly motifs; these motifs serve as glycosaminoglycan attachment sites with two to three heparan sulfate chains and one chondroitin sulfate chain of heterogeneous size (Jha et al. 2009; Yang et al. 2005). These HEK cells were used only for the perlecan expression studies. The expression is controlled by the EBNA-expressing plasmid that is selected for by geneticin (G419). This means that in order to initiate PlnDI expression (which is transcriptionally controlled by the EBV promoter and needs EBNA protein for translation), the cells must be grown under both 20 μg/ml of geneticin and 10 μg/ml of puromycin. Monkey kidney COS-7 cells were purchased from ATCC (Manassas, VA); these cells were used only for the sedimentation studies. COS-7 cells were grown in DMEM supplemented with 10% FBS, glucose, and sodium carbonate, and incubated at 37 °C/5% CO_2. *MuSK*$^{-/-}$ cells, generously provided by Dr. Lin Mei (Medical College of Georgia, Augusta), were maintained in DMEM supplemented with

15% FBS, 1% pyruvate, 2% chick embryo extract, gentamycin sulfate, and interferon-γ, and incubated at 32°C/10% CO_2.

Immunohistochemical Analysis

Slides with frozen cryostat tissue sections of 8-mm thickness were treated with phosphate-buffered saline (PBS) for 10 min at room temperature (RT), and the slides were blocked with 10% goat serum for 1.5 h at RT, and then incubated overnight at 4°C with a goat antibody against ColQ, MuSK, and perlecan (1:50; Santa Cruz Biotechnology, Santa Cruz, CA). The slides were labeled for 1.5 h at RT with a donkey anti-goat IgG fluorescein isothiocyanate (1:200; Santa Cruz Biotechnology), and a rhodamine-conjugated α-Bgt (125 nM; Sigma, St. Louis, MO), and were washed and mounted with ProLong Gold Anti-Fade reagent with 4′,6-diamidino-2-phenylindole (Invitrogen, Grand Island, NY). The tissue was then visualized using a Nikon E-600 fluorescent microscope (Nikon Instruments Inc., Melville, NY). Quantitative analysis of surface extension and intensity of fluorescence was performed using Image-J software. Fluorescence intensity was corrected for background intensity and reported in arbitrary units (Maselli et al., 2010).

Mutational Analysis

Blood from patients and members of the patients' families was used to extract genomic DNA using the QIAmp DNA Blood Kit (Qiagen, Valencia, CA). All 17 coding exons including exon-intron boundaries of the human ColQ gene (GenBank accession number NM_005677.3) and promoter regions were amplified by polymerase chain reaction (PCR) and sequenced on an ABI 3730 DNA Analyzer (Applied Biosystems, Foster City, CA). The sequences were analyzed with BioEdit software to find possible mutations, and sequence variants, whether pathogenic or not, were documented for later analysis. Our institutional review board approved the study. Patients were informed of their rights and the details of the research, and they all signed an informed consent form.

RNA Purification and Transcription Expression

We purified total RNA using 50 mg of muscle from one patient and one control to study the transcription expression of ColQ transcripts. Total RNA was purified using the RNeasy-Plus Mini-kit (Qiagen). One microgram of purified patient and control RNA was reverse transcribed using 500 ng of oligo-dT primers and superscript III reverse transcriptase (Invitrogen). Reverse-transcription PCR (RT-PCR) reactions were performed for each RNA sample, and the PCRs were repeated several times for each RT-PCR. Specific pairs of primers were design to amplify the whole *COLQ* cDNA sequence (Supplementary Table S1). *GAPDH* cDNAs were used as internal standards. Primers for GAPDH were forward: 5′-ATGAATACGGCTACAGCA-3′ and reverse: 5′-GCCCCTCCGTTATTATGG-3′. Amplifications were performed in a Gene Amp PCR System 9700 (Applied Biosystems) using SYBR Green PCR (Applied Biosystems) (Arredondo et al. 2002). Denaturation and amplification of the Taq DNA polymerase were performed at 94°C for 5 min (1 cycle) followed by 30 cycles of denaturation, annealing, and extension of 94°C for 30 s, 60°C for 1 min, and 72°C for 3 min. Standard linear curves were generated for each couple of primers using serial dilutions of the RT reaction. Quantifications were made from cycle threshold

(CT) within these standard curves. Relative expression levels of ColQ mRNAs were determined according to GAPDH levels as an internal control.

Generation of Expression Constructs

Mammalian expression vectors—Total RNA extracted from human muscle was used to prepare *ColQ* cDNA by RT-PCR. The *COLQ* cDNA was cloned from the Human Skeletal Muscle Marathon-Ready™ cDNA (Clontech, Palo Alto, CA) into the pTarget plasmid vector (Promega, Madison, WI). The coding sequence of *COLQ* cDNA was amplified using gene-specific forward (5′-ATGGTTGTCCTGAATCCAATGA-3′) and reverse (5′-TCAGGTGAAGTAGCGGCAGGGC-3′) primers with an amplicon product of 1,367 bp for *COLQ* (NM_005677.3). Human $ACHE_t$ was cloned into pDNA3.1 (Invitrogen) expression vector, kindly provided by Dr. Palmer Taylor (UC San Diego). The p.Gln211*, p.Asp370Asn, p.Cys397Ser, p.Cys400Tyr, p.Tyr404Asp, p.Cys405Phe, and p.Gly423Val mutations were introduced into *ColQ* cDNA using the QuikChange II Site Directed Mutagenesis kit (Stratagene, La Jolla, CA), and transformed into XL1-Blue competent cells. Then the mutant sequence of each construct was confirmed by direct sequencing. The human full-length *MUSK* cDNA construct was purchased from Open Biosystems (Huntsville, AL). The *MUSK* cDNA clone was PCR amplified and subcloned into pcDNA4/HisMax (Invitrogen) expression vector (Maselli et al. 2010).

Expression Studies

Expression in COS cells—COS-7 cells were grown and transfected 24 h after passaging with Lipofectamine 2000 (Invitrogen) according to the manufacturer's protocol, with 19 μg of human $ACHE_T$ cDNA and 19 μg of wild-type or mutant p.Gln211*, p.Asp370Asn, p.Cys397Ser, p.Cys400Tyr, p.Tyr404Asp, p.Cys405Phe, and p.Gly423Val *COLQ* cDNA for each 75-cm^2 flask. The cells were collected 48 h post-transfection and lysed with lysis buffer (50 mM Tris, Ph7.0, 1M NaCl, 0.5% Triton X-100, 0.2 mM EGTA, 2 μg/ml leupetin, and 1 μg/ml pepstatin) for the sedimentation analysis (Ohno et al. 1998). Cells were also transfected with GFP for transfection efficiency.

Sedimentation Analysis

The analysis of the enzyme catalytic molecular forms was performed by linear sucrose density gradient centrifugation. The 5–20% linear sucrose log gradient (P = 1.3 g/ml) centrifugation in lysis buffer was performed in a Beckman SW28 rotor at 25,000 rpm for 21 h at 4°C as described previously, with modifications (Bon et al. 1991). We used 35 cm^2 centrifuge tubes to be able to collect large amounts of A_{12} $AChE_T$ forms per sample. The samples contained 100 μg of COS-7 cell extract and marker proteins with known sedimentation constants, such as alkaline phosphatase (6.1 S) and β-galactosidase (16 S) from *Escherichia coli*, which were included as internal sedimentation standards. Fraction numbers were converted to S values by using the linear relationship between fraction numbers and the positions of the markers in the gradient. The sucrose gradients were fractionated for each sample and AChE esterase activity was determined in the gradient fractions by Ellman assay (Ellman et al. 1961) in the presence of 10^{-4} M of tetraisopropyl pyrophosphoramide (iso-OMPA), an inhibitor of butyrylcholinesterase (Sigma).

Purification of AChE Forms

The isolated sucrose gradient fraction containing the A_{12} AChE forms were purified using HiTrap Heparin HP columns (GE Healthcare, Pittsburgh, PA). Following manufacturer protocol with minor modifications, the fractions were diluted in Tris HCl buffer containing 0.2 M NaCl and loaded onto a 5-ml column. The columns were equilibrated with binding buffer containing 0.2 M NaCl in 10 mM sodium phosphate, pH 7 buffer, and then were washed five times with 5 ml of binding buffer. The A_{12} forms were eluted with 10 mM sodium phosphate with 1 M NaCl. The eluted fractions containing the AChE forms were concentrated with Amicon Ultra-15 centrifugal filters (Millipore) and diluted in Tris-HCl buffer containing 0.2 m NaCl (Kimbell et al. 2004; Kawakami et al. 2011).

Binding assay for quantifying ColQ and MuSK interaction

The Immuno 96-well Maxi-Sorp Plates (Thermo Scientific, Hudson, NH) were coated with 0.15 μg of MuSK protein (Millipore) at 4°C overnight, and incubated with a blocking buffer that contained 50 mM Tris-HCl (pH 7.4), 0.5% bovine serum albumin, 0.5% ovalbumin, and 0.5 M NaCl at RT for 1 hour. The plates were incubated in equal Ellman units of purified A_{12} AChE wild-type or mutant at 4°C for 4 h and then the bound A_{12} forms were quantified by the Ellman method. The plates were washed at least three times with phosphate-buffered saline (Kawakami et al., 2011).

Purification of PlnDI

To purify PlnDI, the HEK-EBNA cells were grown under 10 μg/ml puromycin and 10 μg/ml gentamicin to induce its expression. The cells expressing PlnDI were cultured in 125-cm^2 flasks. Serum-free conditioned medium was collected every other day for 10 days and stored at −20°C. After the filtration of cell debris, the medium was concentrated and partially purified with Amicon-Ultra 15 mL filters with 10K molecular weight cutoff (Millipore). The medium was applied to a diethylaminoethyl-cellulose column (2.5 × 10 cm; Bio-Rad, Hercules, CA), equilibrated with 0.05 M Tris-HCl (pH 8.6), 2 M urea, 0.25 M NaCl, 2.5 mM EDTA, 0.5 mM phenylmethylsulfonyl fluoride (PMSF), and 5 mM benzamidine. After many washes with the equilibration buffer, PlnDI was eluted with 0.5 M NaCl in 0.05 M Tris-HCl (pH 8.6), 2 M urea, 2.5 mM EDTA, 0.5 mM PMSF, and 5 mM benzamidine. PlnDI purity was assessed by 4-20% SDS-PAGE, followed by Western blot analysis with PlnDI-specific antibodies (Yang et al., 2005). Approximately, 40 μg/ml of PlnDI was digested with heparitinases I, II, and III (50 IU/g protein) and chondroitinase AC (1 U/mg protein) prior to electrophoresis.

A_{12} AChE Forms Binding to PlnDI

A dot blotting was used to determine the functional activity of PlnDI to bind A_{12} AChE forms. The PlnDI protein was digested with chondroitinase AC or heparinases I, II, and III for 4 h at 37°C. Three micrograms of undigested or digested PlnDI was blotted onto 0.2 μm nitrocellulose, and subsequently blocked with LI-COR (Lincoln, NE) Odyssey Blocking Buffer for 4 h at 4°C. After washing with blocking buffer, 10 ng of A_{12} AChE was added to each well for binding and incubated overnight at 4°C. The membrane was removed from the blotting apparatus and blocked with 10% goat serum in blocking buffer for 4 h at 4°C,

before incubation in anti-goat ColQ antibody overnight at 4°C. After this incubation, the membrane was washed in washing buffer containing 0.05% Tween 20 in PBS, and incubated with far-red fluorescence secondary antibody donkey anti-goat IRDye 800CW (LI-COR) 1 h at RT. After washing 3 × with washing buffer, the bound antibody was detected using the Odyssey Imaging System (LI-COR) (Yang et al. 2005; Arredondo et al. 2008).

Pull-down Assays

HEK-293 Cell Transfection—HEK293 cells were grown and transfected 24 h after seeding using DharmFECT1 transfection reagent as described previously (Arredondo et al. 2006), with 19 μg of human *MUSK* cDNA and 19 μg of wild-type or *ColQ* mutant cDNA for each 75-cm^2 flask. The cells were co-transfected with human *MUSK* and GFP to verify transfection efficiency. After 48 h post-transfection, the transfected and control cells were lysed with RIPA buffer (Sigma, St. Louis, MO) containing Protease Cocktail Inhibitor (Sigma).

HEK-293-EBNA Cell Transfection—The HEK-293-EBNA cells were grown and transfected 24 h after seeding, with 19 μg $ACHE_T$ cDNA and 19 μg of wild-type or mutant *COLQ* cDNA for each 75-cm^2 flask. The cells expressing PlnDI vector were selected by puromycin, and their expression is controlled by the EBNA promoter that is induced by geneticin (G419, Invitrogen). Thus, to achieve high PlnDI expression, the HEK-293-EBNA cells were grown under geneticin and puromycin (Sigma) (Costell et al. 1997; Yang et al. 2005). After 48 h post-transfection, the cells were lysed with 500 μl RIPA buffer containing 50 μl of Protease Cocktail Inhibitor.

Immunoprecipitation with Sepharose 4 Fast Flow—Both transfected HEK-293 and HEK-293-EBNA cells were harvested by centrifugation at 200*g* for 10 min at 4°C to remove the supernatants, and lysed. The cell lysates were homogenized by sonication in RIPA buffer and protease inhibitors, and centrifuged at 12,000*g* for 10 min at 4°C to remove cell debris. The antibodies present in the cell lysates were removed by adding 100 μl Protein A Sepharose beads to 1 ml of cell lysate and incubating for 1 h at 4°C. The coupling of antigen to antibody was with 500 μl of cell lysates and 5 μg of MuSK or ColQ polyclonal antibody for 2 h at 4°C. The immune complex was precipitated with 100 μl of Protein G Sepharose Fast Flow (GE Healthcare) for 16 h at 4°C, following the manufacturer's protocol (Jungbauer et al. 1989; Amersham Biosciences 2002). The primary antibodies used for immunoprecipitation and Western blots were from different species to prevent detection of the IgG chains in the Western blots.

SDS-PAGE and Western Blot Analysis—The immunoprecipitated protein complexes were quantified using a NanoDrop spectrophotometer (NanoDrop Technologies, Wilmington, DE), with a concentration range from 10 to 50 μg of protein. The protein complex was resuspended with a sample application buffer (1.0 mL of 0.5 M Tris-HCl pH 6.8, 1.9 g ultra-pure urea, and 10% SDS); 20 μg of protein was loaded per sample and separated on a 4–20% SDS-PAGE gradient gel (Bio-Rad), and electroblotted as previously described (Arredondo et al. 2005). The primary antibodies, rabbit anti-MuSK, goat anti-

ColQ, and rabbit anti-perlecan (Santa Cruz Biotechnology), were diluted 1:1,000 in LI-COR Odyssey Blocking Buffer and incubated overnight at 4°C. The secondary antibodies, donkey anti-goat or donkey anti-rabbit IRDye 800CW (LI-COR), were diluted 1:5,000. To normalize for protein content, the housekeeping protein β-actin was visualized in each sample with anti-β-actin monoclonal antibody (1:1,000; Santa Cruz Biotechnology) and with a secondary antibody goat anti-mouse IRDye 600CW (1:5,000; LI-COR). The protein expression was then quantitated using the Odyssey Imaging System (LI-COR).

3-D Culture Matrix BME Assay

3-D culture is an innovative approach for modeling the structural effects in three-dimensional microenvironments. It provides the most standardized BME for use in 3-D culture. Basement membranes are continuous sheets of specialized extracellular matrix that form an interface between endothelial, epithelial, muscle, or neuronal cells and their adjacent stroma (Debnath et al. 2003; Fridman et al. 1990; Hodkinson et al. 2006). The BME is purified from murine Engelbreth-Holm-Swarm (EHS) sarcoma cells. The reconstituted basement membrane is primarily composed of laminin I, collagen IV, nidogen-1 (entactin), and HSPGs, according to the manufacturer (Trevigen, Gaithersburg, MD). The BME protein concentration was quantified by mass spectrometry. With minimal modifications, a 96-well plate was coated with 35 μg of BME distributed as follows for the main proteins: laminin I with 18.84 μg, collagen IV with 6.13 μg, nidogen-1 with 6.48 μg, and HSPGs with 3.54 μg, and incubated at 37°C for 1 h to promote matrix formation. Then, either 100 ng per well of protein from pull-downs or 10 ng per well of A_{12} AChE asymmetric forms from transfected HEK-293 cells with ColQ constructs was added on top of the BME gel matrix and incubated at 4°C for 16 h. The advantage of using cell lysates is that the proteins will be found properly folded to their native structure. To detect the binding of ColQ to the BME matrix, we performed In-Cell Western (ICW) as described in detail elsewhere (Arredondo et al. 2008), using the reagents and equipment from LI-COR Odyssey Blocking Buffer for 1.5 h, and then incubated overnight at 4°C with a ColQ primary antibody. After that, the binding complex was washed and stained for 1 h at RT with a secondary LI-COR IRDye 800CW conjugated donkey anti-goat far-red fluorescent antibody diluted by 1:5,000. The ColQ protein binding was quantified using the LI-COR Odyssey Imaging System.

AChE Assay in BME

The HEK-293 cells were grown in 75-cm^2 flasks, approximately 4×10^6 per flask, and were co-transfected with human 19 μg of *COLQ* and 19 μg *AChE$_T$* constructs per flask to express and produce the heteromeric $AChE_T$ asymmetric forms. After 48 h of transfection, the transfected cells were lysed with buffer containing 50 mM Tris (pH 7.0), 1M NaCl, 0.5% Triton X-100, 0.2 mM EGTA, 2 μg/ml leupeptin, and 1 μg/ml pepstatin. The 10 ng of A_{12} AChE forms or 100 ng of pull-downs per well was incubated on top of the 96-well plate coated with BME as described above and incubated at 4°C overnight to promote the binding of $AChE_T$ asymmetric forms. The plates were washed 3 times for 30 min with PBS to remove the unbond protein. Then, the AChE enzymatic activity was measured in the plates by performing the Ellman assay containing 0.1 M sodium phosphate, pH 8.0, 1 mM EDTA, 75 mM acetylthiocholine iodide as a substrate and 10 mM Ellman reagent (DTNB) with a

150:2:5 ratio. The turnover of AChE enzymatic activity for each mutant was determined by different enzyme concentrations and time points, and by measuring the absorbance at A_{405nm}. The concentration of AChE protein was estimated by enzymatic assay using the turnover number for AChE, 1.45 mmol/min/mg protein, as previously determined by Vigny et al (1978). The stock solution of A_{12} was 0.2 μg/ml.

Sensitive Liquid Chromatography Tandem Mass Spectrometry (LC/MS/MS)

The proteins from the 35 μg BME per lane were separated by SDS-PAGE, the stained bands were cut, and proteins were purified by chloroform-methanol precipitation, which is a useful method for removal of salt and detergents (Wessel and Flugge 1984); the proteins then were proteolytically digested with trypsin into small peptides. The pool of peptides was analyzed using sensitive LC/MS/MS with a Thermo Scientific LTQ linear ion trap mass spectrometer in conjunction with a Paradigm MG4 HPLC (see supplement for details), and the identified peptides were reassembled into proteins (Spivak et al. 2012; Strochlic et al. 2001). The data from the LC/MS/MS were analyzed by using the proteomics software Scaffold version 3.5.1 (Proteome Software Inc., Portland, OR) to visualize and validate the complex MS/MS proteomics experiments. Scaffold 3.5.1 provides a view graphic comparison of protein expression. Scaffold displays a complete, experimental view of the proteins identified in a tandem mass spectrometry analysis. Protein identification results were displayed as probability scores, allowing us to balance the number of proteins and the confidence level of each identification, and validate the identified proteins from LC/MS/MS data. Scaffold uses proven statistical algorithms to calculate the probability that proteins are actually in BME samples (Keller et al. 2002; Nesvizhskii et al. 2003). Another advantage of using LC/MS/MS is that it is possible to quantify the amount of protein from BME samples.

Structural Analysis of COOH-Terminal Domain of ColQ Subunit

The Swiss-PdbViewer (Geneva, Switzerland) V4.1.0 graphics program (Guex and Peitsch 1997) was used for analyzing the position of the identified mutations at the COOH domain of ColQ. Swiss-PdbViewer is an application that provides an interface allowing the analysis of several proteins at the same time (Schwede et al. 2003). The ColQ mutations p.Asp370Asn, p.Cys397Ser, p.Cys400Tyr, p.Tyr404Asp, p.Cys405Phe, and p.Gly423Val were superimposed in order to verify structural alignments, and to identify H-bond changes resulting from the mutated residues in comparison with WT. The amino acid mutations were introduced, and H-bonds and distance changes between atoms were obtained for each mutation. Since there is no available crystallographic structure of ColQ, we provide a theoretical tertiary model of the last 157 residues of ColQ COOH-domain from V298 to T455 (protein sequence: NP_005668.2). The iterative threading assembly refinement (I-TASSER) server (http://zhanglab.ccmb.med.umich.edu/I-TASSER) was used to create the model. The COOH domain has 166 residues with 9 proline in the first half of the domain, and 10 cysteine in the second half of the domain. The later constitutes the cysteine-rich region that includes p.Cys397Ser, p.Cys400Tyr and p.Cys405Phe mutants, and also contains the Myxococcus cysteine-rich repeat, from amino acids 373 to 397. The I-TASSER server is an integrated platform for automated protein structure and function prediction based on the sequence-to-structure-to-function paradigm (Zhang 2008). 3D models are built based on multiple alignments of the sequence homologs, which are also used to predict the secondary

structure using PSIPRED. Assisted by the sequence profile and the predicted secondary structure, the sequence is then threaded through a representative PDB structure library using LOMETS, a server combining seven state-of-the-art threading programs (FUGUE, HHSEARCH, MUSTER, PROSPECT, PPA, SP3 and SPARKS), and iterative TASSER assembly simulations; function insights are then derived by matching the predicted models with the BioLiP protein function database. I-TASSER provided a better homology model than SPARKS, Phye2, and Raptor X servers (Roy et al. 2010, 2012). The homology model can be used for structure-function relationships when the template modeling score (TM-score) is around 0.4 (Zhang and Skolnick 2004). The TM-score is a measure of similarity between two protein structures with different tertiary structures (Zhang and Skolnick. 2005).

Statistical Analysis

All experiments were performed in triplicate and the results were expressed as mean ± standard deviation. Statistical significance was determined using Student's *t* test. Differences were deemed significant if the calculated *p* value was <0.05.

RESULTS

Patients and Mutational Analysis

A total of seven patients from five independent families with AChE deficiency were studied. All patients presented symptoms of weakness and muscle fatigability at birth or shortly thereafter. All patients had respiratory difficulties, usually precipitated by intercurrent infections, and patients 6 and 7 required intermittent mechanical respiratory assistance. None of the patients responded to AChE inhibitors. Except for patient 6 from family 4. The diagnosis in the rest of the families with AChE deficiency was confirmed by muscle biopsy, which included EP AChE staining and electron microscopy of the NMJ. Patients 1 and 2 belonged to an Asian-Caucasian family, patients 3 and 4 belonged to an African American family, patient 5 was conceived by an African American couple and patients 6 and 7 belonged to two unrelated Caucasian families. There was no consanguinity in any of the families. Patients 1 and 2 from family 1 carried mutations p.Gln211* and p.Cys400Tyr; patients 3 and 4 from family 2 carried mutations p.Tyr404Asp, and p.Gly423Val, and a variant p.Asp370Asn; patient 5 from family 3 carried mutation p.Gly423Val and the variant p.Asp370Asn; and patient 6 from family 4 carried mutations c.1082delC and p.Cys397Ser. Finally, patient 7 from family 5 carried mutation p.Cys405Phe and a yet to be identified second pathogenic mutation. Mutations p.Cys397Ser, p.Cys400Tyr, p.Tyr404Asp, p.Cys405Phe and p.Gly423Val are novel, whereas p.Asp370Asn has been reported as a rare polymorphism (rs116373583). In families 2 and 3, the single nucleotide variant p.Asp370Asn and p.Gly423Val were homoallelic. None of the novel mutations were found in 100 control DNA samples. By contrast, p.Asp370Asn was found in one out of 100 DNA control samples. The family tree showing the pattern of segregation and the chromatograms for each of the reported mutations is shown in Fig. S1–S5. A second mutation in *COLQ* accounting for the recessive transmission of deficiency of EP AChE could not be identified in patients 5 and 7. However, sequencing of the promoter region of all patients showed that patient 5 had a heteroallelic combination of p.Gly423Val and a potentially damaging unreported sequence variant in the promoter region (Supplement Section). In patient 7,

sequencing of the promoter region and analysis of transcripts from muscle RNA were unrevealing (Fig. S6–S7).

Expression Studies

1. The COOH-terminal ColQ mutants do not affect the assembly of ColQ with $AChE_T$ to form the asymmetric types of AChE—To investigate the effect of *COLQ* mutants on the assembly of ColQ with *$ACHE_T$*, we co-transfected either WT COLQ or the COLQ mutants— p.Gln211*, p.Asp370Asn, p.Cys397Ser, p.Cys400Tyr, p.Tyr404Asp, p.Cys405Phe or p.Gly423Val—along with WT $AChE_T$ cDNA into heterologous COS-7 cells and analyzed the sedimentation profiles of globular and asymmetric molecular forms of *$ACHE_T$* from the cell lysates by linear sucrose gradients as shown in Fig. 1b. As a negative control, COS cells were transfected only with WT $AChE_T$ cDNA and expressed only G2 and G1 globular forms (data not shown). Co-transfection of $AChE_T$ with p.Gln211*, which predicts the generation of a truncated ColQ protein lacking COOH-terminal domain, produced only G2 and G1 globular forms with a similar sedimentation profile as WT $AChE_T$ expression alone, plus an aberrant M peak. Co-transfection of $AChE_T$ with p.Asp370Asn, p.Cys397Ser, p.Cys400Tyr, p.Tyr404Asp, p.Cys405Phe and p.Gly423Val produced similar sedimentation profiles as WT ColQ co-expressed with $AChE_T$, and contained the asymmetric A_{12}, A_8, and A_4, and the G_4, G_2, and G_1 globular forms displayed in Fig. 1b. The amplitudes of the A_{12} and the G_1 and G_2 peaks are highly variable from transfection to transfection. All mutants had the same protein expression, since they are expressed from the same vector and CMV promoter, and the stability of all the mutants were the same as the wild type (Fig.S8a). High expression levels of ColQ and AChE proteins were demonstrated by Western blots as shown in Fig. 1c, d. Western blot variations of transfection efficiency were normalized by monitoring the expression of β-actin in the immunoblots.

2. The COOH-terminal COLQ mutants do not affect the binding of ColQ to perlecan—To examine the interaction of WT and ColQ mutants to perlecan, special HEK-EBNA cells were induced to overexpress PlnDI, and were subsequently co-transfected with $AChE_T$ and WT or mutant ColQ. Our experiments showed high expression of PlnDI of at least 100-fold over the endogenous perlecan (Fig. S8b), which is similar to high expression of PlnDI observed by other laboratories (Costell et al. 1997; Jha et al. 2009; Yang et al. 2005). Initially, cells expressing both PlnDI and $AChE_T$ and ColQ proteins were lysed after 48 h post-transfection and immunoprecipitated with ColQ antibody. The immunoprecipitation showed a strong interaction between WT and ColQ mutants with PlnDI (Fig. 2a). These results show that PlnDI protein interacts with the ColQ subunit, and that the identified COOH-terminal domain mutations do not alter the previously demonstrated interaction between perlecan heparan sulfate chains and the two HSPG domains in the ColQ subunit (Deprez et al. 2000). To confirm the interaction of ColQ subunits with PlnDI, we used a quantitative dot blot assays to measure the bindings of purified A_{12} forms of WT and ColQ mutants with purified PlnDI. Briefly, PlnDI was immobilized on nitrocellulose in its native form or after digestion with heparinases I, II, and III or chondroitinase AC. Binding of A_{12} forms to PlnDI was detected with ColQ antibodies. Figure 2b shows a representative dot blot showing A_{12} forms binding to PlnDI. No binding

was observed in areas PlnDI and digested with glycosaminoglycan enzymes. In contrast, A_{12} forms bound strongly to intact, chondroitinase AC-digested, but not heparinase-digested, PlnDI. Figure 2c summarizes the analyses of this data. The Fig.2d shows a summary of the dot-blot assays, where wild-type and mutants show the same interaction between PlnDI and ColQ. In summary, these results confirm strong interaction between the A_{12} forms and PlnDI and that this interaction is dependent on the heparan sulfate attachments of perlecan. Furthermore, our study shows no difference between the ability of wild-type and mutant A_{12} forms to interact with PlnDI.

3. The COOH-terminal COLQ mutants reduce binding of ColQ to MuSK— Initially, to assess the interaction of COLQ to MuSK, HEK cells were co-transfected with human WT or *ColQ* mutants and WT MUSK; the high expression of MuSK protein was confirmed by Western blot (Fig. S8c). The transfected cells were harvested after 48 h post-transfection, and the protein complex was immunoprecipitated with rabbit anti-MuSK antibody to study the interaction of ColQ with MuSK. The protein complex immunoblotted with goat antibody against ColQ showed a strong interaction between MuSK and WT ColQ. However, compared with WT ColQ, the mutants showed only a mild decrease of affinity to MuSK, which was reduced by 1.5% for p.Asp370Asn, 6.7% for p.Cys397Ser, 5% for p.Cys400Tyr, 7.4% for p.Tyr404Asp, and 16.8% for p.Gly423Val, as shown in Fig. 3a. In comparison with WT *COLQ*, the reduction was only significant ($p<0.05$) only for p.Gly423Val. To further investigate the interaction of ColQ and MuSK, we next studied whether the COOH-terminus ColQ mutations had an effect on the interaction of ColQ and MuSK using an overlay binding assay (Nakata et al. 2013). The plates were coated with purified MuSK, and incubated with the AChE A_{12} forms. The Ellman assay was used to quantify the A_{12} forms binding to MuSK. AChE enzymatic activity of the ColQ mutants were reduced compared to wild-type as follow: 15% for p.Asp370Asn and 18% for p.Cys397Ser, and the reduction was significant ($p<0.05$) for p.Cys400Tyr, p.Tyr404Asp, p.Cys405Phe and p.Gly423Val with 39, 45, 36 and 0.51% respectively, as shown in Fig. 3b. The results indicate that the mutations decreased the binding affinity between ColQ and MuSK proteins.

4. The *COOH*-terminal COLQ mutants reduced binding of ColQ to basement membrane extract—We hypothesized that the mechanism responsible for the patients' deficiency of AChE at the EP is due to the inability of ColQ mutants to anchor the enzyme properly to the basal membrane. We assumed the possibility that not only MuSK and perlecan proteins are involved in the binding of ColQ, but the binding may also depend on other molecules. To test this hypothesis, we first quantified the protein composition of BME by mass spectrometry—BME is primarily composed of laminin I (54% of structural proteins), collagen IV (17%), nidogen-1 (19%), and HSPGs (10%). Initially, the interaction of ColQ with the BME matrix was examined by using cell lysates from transfected cells with wild-type and mutant ColQ, and analyzed with the ICW technique and ColQ antibody. Our results demonstrated that WT ColQ showed the strongest interaction to BME, 100%, and that the mutants displayed varied degrees of reduced binding affinity to BME. In comparison with the WT, the percentage of interaction with the BME was 96.6% for p.Asp370Asn, 96.2% for p.Cys397Ser, 95.8% for p.Tyr404Asp, 94.6% for p.Cys400Tyr,

and 80.1% for p.Gly423Val, which had the lowest binding affinity to BME ($P < 0.05$), data not shown. Finally, to further investigate the binding of ColQ to the BME, the purified A_{12} forms were overlaid on the BME. The binding of ColQ to BME was performed using ICW, and analyzed by measuring the fluorescence of ColQ antibody bound to the BME (Fig. 4a). Mutants p.Asp370Asn and p.Cys397Ser had the lowest interaction reduction with 13 and 14% respectably, and 24% for p.Cys400Tyr ($p<0.05$), 31% for p.Tyr404Asp ($p<0.05$), 33% for p.Cys405Phe ($p<0.05$), and p.Gly423Val has the highest reduction with 46% ($p<0.05$). All were significantly lower than that of WT ColQ as shown in Fig. 4b.

5. The COOH-terminal COLQ mutants reduced the activity of AChE bound to basal membrane extracts—To study the ability of COLQ mutants to anchor the enzyme at the basal membrane, we tested the AChE enzymatic activity on BME-coated plates with the Ellman assay. First, the lysates from transfected HEK-293 cells with human WT $ACHE_T$ cDNA and WT or mutant ColQ cDNA were harvested after 48-h post-transfection and assayed for AChE esterase activity. The lysates from transfected cells with WT AChE cDNA and p.Asp370Asn, p.Cys397Ser, p.Cys400Tyr, p.Tyr404Asp, p.Cys405Phe, or p.Gly423Val were tested first for their AChE enzymatic activity by mixing 0.5 μg of the cell lysates with a 150:2:5 ratio of reaction buffer, substrate, and Ellman reagent, respectively, in a 96-well plate. Our data showed that $AChE_T$ tetramers attached to the ColQ mutant trimer had the same AChE esterase activity as the WT ColQ subunit attached to $AChE_T$ catalytic subunit, data not shown. To quantify the AChE enzymatic activity in solution, we used purified A_{12} forms, and measured the enzyme activity using the Ellman assay (Fig. 5). The results were the same as described above: the COOH-terminus ColQ mutations did not affect the enzymatic efficiency.

Next, the AChE enzymatic activity was tested again, but this time only the activity of the enzyme bound to BME-coated plates was measured. Initially, transfected cell lysates were incubated with BME- coated plates overnight at 4°C, and the unbound $AChE_T$ asymmetric forms were washed before performing the enzymatic reaction. The esterase enzymatic activity was monitored by measuring the absorbance of each sample at $A_{405\ nm}$. Consistent with our previous results, our data showed that WT ColQ subunit bound to the BME had the strongest AChE enzymatic activity (100%), while esterase activity of the mutants was p.Asp370Asn, 90.8% for p.Cys397Ser, p.Tys404Asp, 89% for p.Cys405Phe, 86.5% for p.Cys400Tyr, and p.Glyc423Val, data not shown. Subsequently, the purified A12 AChE forms were used to accurately quantify the interaction of ColQ mutants to BME. The data showed that p.Asp370Asn and p.Cys397Ser mutants have enzymatic activity of 93 and 91% respectively. The AChE enzyme activity was 75% for p.Cys400Tyr, 64% for p.Tyr404Asp and 68% for p.Cys405Phe; the highest reduction was with p.Gly423Val with 46%. All the reductions were significant ($P < 0.05$), except for those of p.Asp370Asn and p.Cys397Ser mutants, as shown in Fig. 6; the globular AChE forms were used as a negative control.

6. Identification of proteins from basal membrane extracts by sensitive tandem mass spectrometry—BME samples were purified from murine EHS sarcoma cells. The proteins of BME samples were analyzed using sensitive LC/MS/MS. The data from the LC/MS/MS were analyzed using the proteomics software Scaffold 3.5.1 to

visualize and validate the complex LC/MS/MS proteomics experiments. The Scaffold data analysis identified a total of 30 proteins, where laminins such as α1, γ1, and β1 subunits were not only the most abundant proteins but also the largest number of proteins identified. Laminin subunit α1 was the most abundant protein, followed by laminin I with 54%, nidogen-1 with 19%, collagen IV with 17%, and HSPG 2 (perlecan) with only 10%. LC/MS/MS quantification for 10 μg of BME used the following concentrations: laminin I, 5.4 μg; collagen IV, 1.7 μg; nidogen-1, 1.9 μg; and HSPGs, 1.0 μg. The results from the most abundant 17 proteins are described in Table 1, where the top proteins are the most abundant and the bottom proteins are the least abundant.

7. Structural analysis of ColQ COOH-terminal domain—Since a crystallographic structure of ColQ protein is not available; we designed one tertiary structure by using only the last 157 amino acids of the COOH-domain of human ColQ from V298 to T455 with the I-TASSER server to generate the coordinates of a full-length 3D model of the ColQ-COOH domain (Fig. 7). All the mutated residues occurred in the coil secondary structure. The structure has the C-terminal trimerization domain from residues 294–372, and the cysteine-rich domain from residues 375–451 (Fig.S9a), which includes p.Cys397Ser, p.Cys400Tyr and p.Cys405Phe. The ColQ cysteine-rich domain corresponds to the PD036938 (ProDom database) and is supposed to form disulfide bonds, which is similar to the peptide motif Myxococcus cysteine-rich repeat (IPR011936), which includes p.Cys397Ser mutation (Fig.S9a). The disulfide bonds are linked by the coupling of two thiol groups of Cys400 and Cys405, which belong to the cysteine-rich domain (Fig.S9a). To validate the ColQ protein structure, fragment-guided MD simulations (FG-MD) and ModRefiner (high-resolution protein structure refinement) were used for high-resolution and atomic-level protein structure refinements. The FG-MD and ModRefiner are template-based modeling, representing the most accurate method in protein structure prediction. Our predicted ColQ model has a TM score of 0.9944 and a root mean squared deviation of 0.352. TM score is to assess the quality of protein structure; a TM score >0.5 indicates a model of correct topology. Our model has a C score of -4.5; C score is a confidence score for estimating the quality of predicted models and the prediction of ColQ trimerization domain match with the triple-helix organization. The six human mutations p.Asp370Asn, p.Cys397Ser, p.Cys400Tyr, p.Tyr404Asp, p.Cys405Phe, and p.Gly423Val were introduced into the COOH-terminal domain as shown in Fig. 7. To understand how each of the mutations affected the ColQ protein tertiary structure, we studied how each mutation residue altered the electrostatic dipole-dipole interaction of the hydrogen bonds (H-bonds) in the COOH-terminal domain. In Figs. 8 and S10, we describe in more detail how the ColQ mutations affect normal hydrogen bonding interactions and the folding of the COOH-terminal domain tertiary structure. Because the residue mutations usually affect the conformation of the residues in the neighborhood, Table 2 lists the H-bonds before and after the residue mutations based on the modeled ColQ structure. A summary of the hydrogen bonding interaction changes is described in Table 2, where the number of H-bonds lost, changed, or gained for each point mutation is shown. The data demonstrated that p.D370N mutation produces the least disruptive structural change, because aspartic acid 370 (D370) is a negatively charged polar residue that changes into asparagine 370 (N370), an amide uncharged polar residue (Fig.8a–b). On the other hand, the p.Gly423Val shows a more

disruptive structural change because glycine 423 (G423) is an aliphatic hydrophobic residue; the absence of a side chain is substituted with a hydrogen and changes to valine 423 (V423), a structural aliphatic hydrophobic residue. *p.Gly423Val* is the mutation that creates more damage to the ColQ tertiary structure, because the conserved glycine changing to any other amino acid, like valine, is destabilizing and could have an impact on ColQ conformation and stability; it also creates two new H-bonds, as shown in Fig. 8i, j and Table 2.

DISCUSSION

The data presented here show that single point mutations in the COOH-terminal domain of the ColQ subunit do not prevent the assembly of ColQ with $AChE_T$. However, they disrupt the interaction of ColQ with the basal membrane, which is critical for the accumulation of asymmetric $AChE_T$ at the NMJ. We also provide biochemical evidence that PlnDI plays a crucial role in the interaction with the ColQ subunit at the BL. We also have confirmed that ColQ interacts with MuSK through its carboxyl domain, because COOH-terminal ColQ mutants disrupt the interaction of ColQ with MuSK. Thus, the localization and accumulation of $AChE_T$ at the NMJ rely on specific molecular interactions between ColQ and proteins of the BL. As expected with ColQ's potential multiple domains, it can possibly interact with other proteins. For example, Vigny's group showed that ColQ can interact with other molecules in vitro, including collagens I and V and laminin; other groups also found interaction with liposomes (Cohen and Barenholz 1984) and with collagenous proteins from Torpedo extracellular matrix extract (Casanueva et al. 1998).

Several lines of evidence implicate perlecan in the anchoring of the collagen-tailed AChE to the NMJ, including colocalization of perlecan with AChRs and AChE at the NMJ in vivo and in cultured muscle cells (Maselli et al. 2012; Massoulié and Millard 2009; Peng et al. 1999; Rossi and Rotundo 1996; Rotundo et al. 1997, 2005), absence of AChE clusters at the NMJ in perlecan null mice (Arikawa-Hirasawa et al. 2002), and binding of asymmetric AChE species to immobilized perlecan in vitro (Peng et al. 1999).

In this study the use of special HEK-293 cells expressing only PlnDI allowed us to verify by a pull-down assay a strong interaction of perlecan with ColQ and to assume that this interaction takes place between the heparan sulfate side chains of PlnDI and the two HSPGB sites of ColQ. The use of PlnDI instead of the whole perlecan protein was appropriate for our experimental condition, and indeed this approach has been used by other researchers assessing the interaction of this multidomain molecule with other proteins. Rupert Timpl's group did many experiments of protein binding, analyzing the different domains of extracellular membrane proteins and their interactions, including PlnDI (Costell et al. 1997); they always used the recombinant domains, not the whole molecule. Thus, our findings are consistent with those of previous experiments (Casanueva et al. 2008) that the interaction between HSPG of PlnDI and ColQ contributes to the binding of asymmetric AChE forms to the BL, and that the mutations of the COOH-terminus domain do not impair the interaction. Nevertheless, these experiments cannot exclude that interactions between the protein cores of PlnDI and ColQ could occur. However, since we found several COOH-terminal mutants, which caused severe human deficiency of EP AChE that did not alter the interaction of perlecan with ColQ, it follows that the interaction of perlecan to ColQ is necessary but not

sufficient for anchoring ColQ to the synaptic BL. Therefore, the attachment of the asymmetric forms of AChE to the BL at the NMJ is likely to involve additional protein interactions. The perlecan binding to the ColQ triple-helical structure requires the positively charged residues of the HSPGB sites to be exposed, which takes placed after the formation of the triple-helical structure (Deprez and Inestrosa 1995).

Previous studies have shown that ColQ binds through its COOH terminus to MuSK (Cartaud et al. 2004; Nakata et al. 2013; Sigoillot et al. 2010), and we confirmed these findings. The interaction of ColQ with MuSK is important because, in contrast with perlecan, MuSK expresses exclusively at the NMJ and, therefore it may confer ColQ synaptic specificity. The importance of MuSK protein was further demonstrated by experiments that showed that when MuSK was transfected into muscle cells it induced the formation of AChE clusters (Jones et al. 1999; Antolik et al. 2006). However, in our study we found that COOH-terminal ColQ mutants cause more impairment of the binding of ColQ to MuSK than to BME, which does not have detectable MuSK. This observation, coupled with the recently reported finding of normal AChE expression at the EPs of patients with anti-MuSK myasthenia possessing serum antibodies that block the binding of ColQ to MuSK (Kawakami et al. 2011), suggests that the binding of COOH-terminal domain of ColQ to the BL is in part independent of MuSK. Recently, *COLQ* mutations in the COOH-terminal domain showed that the mutations impair this interaction between ColQ and MuSK by in vitro and in vivo assays (Nakata et al. 2013), and our findings are in line with those results.

The reduced interaction of COOH-terminal ColQ mutants with BME in our study is consistent with previous observations of Kimbell et al. (2004) that several human COOH-terminal COLQ mutations transplanted into heterologous frog NMJ were insertion incompetent. Although the technique that was used in our study is also an overlay assay, in comparison with the method described by Kimbell et al., it is considerably simpler and has the additional advantage of providing quantitative analysis.

In search for additional partners of ColQ, the BME samples were analyzed by mass spectrometry, and quantified the proteins that were used for the overlay assay. We found that four were the most abundant and relevant proteins for the BL: laminin-1, nidogen-1, collagen IV, and perlecan. Importantly, the study showed no evidence of MuSK; this was confirmed by immunoblotting of the BME (data not shown). The absence of MuSK was not completely unexpected since the BME is purified from a tumoral cell line that includes no synaptic connections. Nevertheless, the fact that the COOH-terminal mutations that were tested did not affect interaction of ColQ to perlecan, but still altered the interaction of ColQ to BME, suggests that in addition to MuSK the COOH-terminal domain of ColQ may interact with other proteins of the BL.

Finally, The I-TASSER server helped to develop the full-length tertiary model of the ColQ-COOH domain. The model predicts not only the ColQ trimerization but also the cysteine-rich domain and the formation of disulfide bonds, which are important in the folding and stability of the protein. The structural analysis also provided an invaluable biochemical tool to understand why single point mutations could have such contrasting effects on the ability of ColQ self-attachment into the BL. At both ends of the spectrum, the ColQ mutations

analyzed in this study are p.Asp370Asn, which produces the least disrupting effect, and p.Gly423Val, which results in the most disrupting effect on ColQ binding to BL. At first glance, there is an apparent reason for the difference: since p.Asp370Asn involves a change of aspartic acid with a negatively charged side chain to asparagine with an uncharged amide side chain, this mutation involves two amino acids of similar side chain size. This change would be less damaging than p.Gly423Val, which involves a change of one aliphatic hydrophobic amino acid with no side chain to a larger and bulky aliphatic amino acid with a hydrophobic uncharged side chain. Consequently, modeling these mutations revealed that while p.Asp370Asn involves a change between two residues of similar mass size, p.Gly423Val involves a change from the small glycine to larger valine residue. It is known that glycine substitutions within a triple helix are destabilizing (Brodsky et al. 2008), and valine is one of the most destabilizing residues, whereas glycine is a unique conserved residue that can reside in parts of protein structures that are forbidden to all other residues (Brodsky and Persikov 2005), like tight protein turns, and therefore is more likely to have an impact to disrupt hydrogen bonding interactions and the proper folding and stability of the COOH terminus of ColQ. But if the glycine substitution occurs in a region that is not triple-helical, then the consequences could also lead to pathological conditions in non-fibrillar collagens. For example, a glycine replacement by a valine at one site in Type IV collagen of α5 chain leads to Alport syndrome (Hudson et al. 2003).

In conclusion, we reported here the molecular effects of missense COOH-terminal COLQ mutations causing human congenital deficiency of EP AChE. While these mutations neither abolish the assembly of ColQ with AChE nor hinder the interaction of ColQ with perlecan, each mutation disrupts the interaction of ColQ with MuSK, and with BME in diverse degrees. It is feasible to expect that ColQ domains that are changed from its normal and stable molecular structures are probable sites for interaction with other proteins, supporting structural flexibility and specificity. Thus, our data confirmed that the attachment of ColQ to the BL involves two different sites of interactions: one through MuSK, which may confer synaptic localization specificity, and the other one through perlecan, which may provide structural stability, as shown in Fig. 9.

Supplementary Material

Refer to Web version on PubMed Central for supplementary material.

Acknowledgments

We thank Dr. Robert Fairclough and Dr. Richard Richman for critical reading of the manuscript, Dr. Palmer Taylor from UC-San Diego for AChE clone, and Dr. Mary C. Farach-Carson from Rice University for the HEK cells expressing perlecan domain I, and Dr. Samuel Ignacio Pascual Pascual, Madrid, Spain, for sharing one of his studied families with us. This work was supported by National Institutes of Health grant RO1NS049117-01 to RAM.

References

Amershan Biosciences. Affinity Chromatography Handbook, Principles and Methods, Code No. 18-1022-29. 2002.

Antolik C, Catino DH, Resneck WG, Bloch RJ. The tetratricopeptide repeat domains of rapsyn bind directly to cytoplasmic sequences of the muscle-specific kinase. Neuroscience. 2006; 141:87–100. [PubMed: 16675143]

Arikawa-Hirasawa E, Rossi SG, Rotundo RL, Yamada Y. Absence of acetylcholinesterase at the neuromuscular junctions of perlecan-null mice. Nat Neurosci. 2002; 5:119–123. [PubMed: 11802174]

Arredondo J, Chernyavsky AI, Jolkovsky DL, Pinkerton KE, Grando SA. Receptor-mediated tobacco toxicity: acceleration of sequential expression of α5 and α7 nicotinic receptor subunits in oral keratinocytes exposed to cigarette smoke. FASEB J. 2008; 22:1356–1368. [PubMed: 18450646]

Arredondo J, Chernyavsky AI, Karaouni A, Jolkosky DL, Pinkerton KE, Grando SA. Receptor-mediated tobacco toxicity: cooperation of the Ras/Raf-1/MEK1/ERK and JAK-2/STAT-3 pathways downstream of alpha7 nicotinic receptor in oral keratinocytes. FASEB J. 2006; 20:2093–2101. [PubMed: 17012261]

Arredondo J, Chernyavsky AI, Webber RJ, Grando SA. Biological effects of SLURP-1 on human keratinocytes. J Investig Dermatol. 2005; 125:1236–1241. [PubMed: 16354194]

Arredondo J, Nguyen VT, Chernyavsky AI, Bercovich D, Orr-Urtreger A, Kummer W, Lips K, Vetter DE, Grando SA. Central role of alpha7 nicotinic receptor in differentiation of the stratified squamous epithelium. J Cell Biol. 2002; 59:325–336. [PubMed: 12391028]

Bon S, Ayon A, Leroy J, Massoulié J. Trimerization domain of the collagen tail of acetylcholinesterase. Neurochem Res. 2003; 28:523–535. [PubMed: 12675141]

Bon S, Coussen F, Massoulie J. Quaternary associations of acetylcholinesterase. II. The polyproline attachment domain of the collagen tail. J Biol Chem. 1997; 272:3016–3021. [PubMed: 9006950]

Bon S, Rosenberry TL, Massoulié J. Amphiphilic, glycophosphatidylinositol-specific phospholipase C (PI-PLC)-insensitive monomers and dimers of acetylcholinesterase. Cell Mol Neurobiol. 1991; 11:157–172. [PubMed: 1849452]

Brodsky B, Shah NK. Protein motifs. 8. The triple-helix motif in proteins. FASEB J. 1995; 9:1537–1546. [PubMed: 8529832]

Brodsky B, Persikov AV. Molecular structure of the collagen triple helix. Adv Protein Chem. 2005; 70:301–339. [PubMed: 15837519]

Brodsky B, Thiagarajan G, Madhan B, Kar K. Triple-helical peptides: an approach to collagen conformation, stability, and self-association. Biopolymers. 2008; 89:345–353. [PubMed: 18275087]

Cartaud A, Strochlic L, Guerra M, Blanchard B, Lambergeon M, Krejci E, Cartaud J, Legay C. MuSK is required for anchoring acetylcholinesterase at the neuromuscular junction. J Cell Biol. 2004; 165:505–515. [PubMed: 15159418]

Casanueva OI, Deprez P, García-Huidobro T, Inestrosa NC. At least two receptors of asymmetric acetylcholinesterase are present at the synaptic basal lamina of Torpedo electric organ. Biochem Biophys Res Commun. 1998; 250:312–317. [PubMed: 9753626]

Cohen R, Barenholz Y. Characterization of the association of Electrophorus electricus acetylcholinesterase with sphingomyelin liposomes. Relevance to collagen-sphingomyelin interactions. Biochim Biophys Acta. 1984; 778:94–104. [PubMed: 6498189]

Costell M, Mann K, Yamada Y, Timpl R. Characterization of recombinant perlecan domain I and its substitution by glycosaminoglycans and oligosaccharides. Eur J Biochem. 1997; 243:115. [PubMed: 9030729]

Debnath J, Muthnuswany SK, Brugge JS. Morphogenesis and oncogenesis of MCF-10A mammary epithelial acini grown in the three-dimensional basement membrane cultures. Methods. 2003; 30:256–268. [PubMed: 12798140]

Deprez P, Doss-Pepe E, Brodsky B, Inestrosa NC. Interaction of the collagen-like tail of asymmetric acetylcholinesterase with heparin depends on triple-helical conformation, sequence and stability. Biochem J. 2000; 350:283–290. [PubMed: 10926855]

Deprez P, Inestrosa NC, Krejci E. Two different heparin-binding domains in the triple-helical domain of ColQ, the collagen tail subunit of synaptic acetylcholinesterase. J Biol Chem. 2003; 278:23233–23242. [PubMed: 12684510]

Deprez PN, Inestrosa NC. Two heparin-binding domains are present on the collagenic tail of asymmetric acetylcholinesterase. J Biol Chem. 1995; 270:11043–11046. [PubMed: 7744733]

Dvir H, Harel M, Bon S, Liu WQ, Vidal M, Garbay C, Sussman JL, Massoulie J, Silman I. The synaptic acetylcholinesterase tetramer assembles around a polyproline II helix. EMBO J. 2004; 23:4394–4405. [PubMed: 15526038]

Ellman GL, Courtney KD, Andres V, Feathersone RM. A new and rapid colorimetric determination of acetylcholinesterase activity. Biochem Pharmacol. 1961; 7:88–95. [PubMed: 13726518]

Engel AG, Ohno K, Sine SM. Sleuthing molecular targets for neurological diseases at the neuromuscular junction. Nat Rev Neurosci. 2003; 4:339–352. [PubMed: 12728262]

Engel J, Prockop DJ. The zipper-like folding of collagen triple helices and the effects of mutations that disrupt the zipper. Annu Rev Biophys Chem. 1991; 20:137–152.

Feng G, Krejci E, Molgo J, Cunningham JM, Massoulie J, Sanes JR. Genetic analysis of collagen Q: roles in acetylcholinesterase and butyrylcholinesterase assembly and in synaptic structure and function. J Cell Biol. 1999; 144:1349–1360. [PubMed: 10087275]

Fridman R, Giaccone G, Kanemoto T, Martin GR, Gazdar AF, Mulshine JL. Reconstituted basement membrane (matrigel) and laminin can enhance the tumorigenicity and the drug resistance of small cell lung cancer cell lines. Proc Natl Acad Sci U S A. 1990; 87(17):6698–6702. [PubMed: 2168554]

Guex N, Peitsch MC. SWISS-MODEL and the Swiss-PdbViewer: an environment for comparative protein modeling. Electrophoresis. 1997; 18:2714–2723. [PubMed: 9504803]

Hall ZW. Multiple forms of acetylcholinesterase and their distribution in endplate and non-endplate regions of rat diaphragm muscle. J Neurobiol. 1973; 4:343–361. [PubMed: 4724813]

Hodkinson PS, Elliott T, Wong WS, Rintoul RC, Mackinnon AC, Haslett C, Sethi T. ECM overrides DNA damage-induced cell cycle arrest and apoptosis in small-cell lung cancer cells through beta1 integrin-dependent activation of PI3-kinase. Cell Death Differ. 2006; 13(10):1776–1788. [PubMed: 16410797]

Hudson BG, Tryggvason K, Sundaramoorthy M, Neilson EG. Alport's syndrome, Goodpasture's syndrome, and type IV collagen. N Engl J Med. 2003; 348:2543–2556. [PubMed: 12815141]

Ishigaki K, Nicolle D, Krejci E, Leroy JP, Koenig J, Fardeau M, Eymard B, Hantaï D. Two novel mutations in the COLQ gene cause endplate acetylcholinesterase deficiency. Neuromuscul Disord. 2003; 13:236–244. [PubMed: 12609505]

Jha AK, Yang W, Kirn-Safran CB, Farach-Carson MC, Jia X. Perlecan domain I-conjugated, hyaluronic acid-based hydrogel particles for enhanced chondrogenic differentiation via BMP-2 release. Biomaterials. 2009; 30:6964–6975. [PubMed: 19775743]

Jones G, Moore C, Hashemolhosseini S, Brenner HR. Constitutively active MuSK is clustered in the absence of agrin and induces ectopic postsynaptic-like membranes in skeletal muscle fibers. J Neurosci. 1999; 19:3376–3383. [PubMed: 10212297]

Jungbauer A, Tauer C, Reiter M, Purtscher M, Wenisch E, Steindl F, Buchacher A, Katinger H. Comparison of protein A, protein G and copolymerised hydroxyapatite for the purification of human monoclonal antibodies. J Chromatogr. 1989; 476:257–268. [PubMed: 2777978]

Katz B, Miledi R. The measurement of synaptic delay, and the time course of acetylcholine release at the neuromuscular junction. Proc R Soc Lond B Biol Sci. 1965; 161:483–496. [PubMed: 14278409]

Katz B, Miledi R. The binding of acetylcholine to receptors and its removal from the synaptic cleft. J Physiol (Lond). 1973; 231:549–574. [PubMed: 4361216]

Keller A, Nesvizhskii AI, Kolker E, Aebersold R. Empirical statistical model to estimate the accuracy of peptide identifications made by MS/MS and database search. Anal Chem. 2002; 74:5383–5392. [PubMed: 12403597]

Kawakami Y, Ito M, Hirayama M, Sahashi K, Ohkawara B, Masuda A, Nishida H, Mabuchi N, Engel AG, Ohno K. Anti-MuSK autoantibodies block binding of collagen Q to MuSK. Neurology. 2011; 77:1819–1826. [PubMed: 22013178]

Kimbell LM, Ohno K, Engel AG, Rotundo RL. C-terminal and heparin-binding domains of collagenic tail subunit are both essential for anchoring acetylcholinesterase at the synapse. J Biol Chem. 2004; 279:10997–11005. [PubMed: 14702351]

Krejci E, Coussen F, Duval N, Chatel JM, Legay C, Puype M, Vandekerckhove J, Cartaud J, Bon S, Massoulié J. Primary structure of a collagenic tail peptide of Torpedo acetylcholinesterase: co-expression with catalytic subunit induces the production of collagen-tailed forms in transfected cells. EMBO J. 1991; 10:1285–1293. [PubMed: 1840520]

Legay C. Why so many forms of acetylcholinesterase? Microsc Res Tech. 2000; 49:56–72. [PubMed: 10757879]

Legay C, Huchet M, Massoulie J, Changeux JP. Developmental regulation of acetylcholinesterase transcripts in the mouse diaphragm: alternative splicing and focalization. Eur J Neurosci. 1995; 7:1803–1809. [PubMed: 7582132]

Legay C, Huchet M, Massoulié J, Changeux JP. Developmental regulation of acetylcholinesterase transcripts in the mouse diaphragm: alternative splicing and focalization. Eur J Neurosci. 1995; 7:1803–1809. [PubMed: 7582132]

Li Y, Camp S, Rachinsky TL, Getman D, Taylor P. Gene structure of mammalian acetylcholinesterase. Alternative exons dictate tissue-specific expression. J Biol Chem. 1991; 266:23083–23090. [PubMed: 1744105]

Li Y, Camp S, Taylor P. Tissue-specific expression and alternative mRNA processing of the mammalian acetylcholinesterase gene. J Biol Chem. 1993; 268:5790–5797. [PubMed: 8449945]

Maselli RA, Arredondo J, Cagney O, Anderson JA, Williams C, Soliven B. MUSK tyrosine kinase domain mutations causing congenital myasthenia syndrome. Hum Mol Genet. 2010; 19:2370–2379. [PubMed: 20371544]

Maselli RA, Arredondo J, Ferns MJ, Wollmann RL. Synaptic basal lamina-associated congenital myasthenic syndromes. Ann N Y Acad Sci. 2012; 1275:36–48. [PubMed: 23278576]

Massoulié J, Anselmet A, Bon S, Krejci E, Legay C, Morel N, Simon S. Acetylcholinesterase: C-terminal domains, molecular forms and functional localization. J Physiol Paris. 1998; 92:183–190. [PubMed: 9789805]

Massoulié J, Anselmet A, Bon S, Krejci E, Legay C, Morel N, Simon S. The polymorphism of acetylcholinesterase: post-translational processing, quaternary associations and localization. Chem Biol Interact. 1999; 119–120:29–42.

Massoulié J, Millard CB. Cholinesterases and the basal lamina at vertebrate neuromuscular junctions. Curr Opin Pharmacol. 2009; 9:316–325. [PubMed: 19423392]

Massoulie J, Pezzementi L, Bon S, Krejci E, Vallette FM. Molecular and cellular biology of cholinesterases. Prog Neurobiol. 1993; 41:31–91. [PubMed: 8321908]

McLaughlin SH, Bulleid NJ. Molecular recognition in procollagen chain assembly. Matrix Biol. 1998; 16:369–377. [PubMed: 9524357]

Nakata T, Ito M, Azuma Y, Otsuka K, Noguchi Y, Komaki H, Okumura A, Shiraishi K, Masuda A, Jun Natsume, Kojima S, Ohno K. Mutations in the C-terminal domain of ColQ in endplate acetylcholinesterase deficiency compromise ColQ MuSK interaction. Hum Mutat. 201310.1002/humu.22325

Nesvizhskii AI, Keller A, Kolker E, Aebersold R. A statistical model for identifying proteins by tandem mass spectrometry. Anal Chem. 2003; 75:4646–4658. [PubMed: 14632076]

Ohno K, Brengman J, Tsujino A, Engel AG. Human endplate acetylcholinesterase deficiency caused by mutations in the collagen-like tail subunit (ColQ) of the asymmetric enzyme. Proc Natl Acad Sci U S A. 1998; 95:9654–9659. [PubMed: 9689136]

Ohno K, Engel AG, Brengman JM, Shen XM, Heidenreich F, Vincent A, Milone M, Tan E, Demirci M, Walsh P, Nakano S, Akiguchi I. The spectrum of mutations causing endplate acetylcholinesterase deficiency. Ann Neurol. 2000; 47:162–170. [PubMed: 10665486]

Peng HB, Xie H, Rossi SG, Rotundo RL. Acetylcholinesterase clustering at the neuromuscular junction involves perlecan and dystroglycan. J Cell Biol. 1999; 145:911–921. [PubMed: 10330416]

Prockop DJ, Kivirikko KI. Collagens: molecular biology, diseases, and potentials for therapy. Annu Rev Biochem. 1995; 64:403–434. [PubMed: 7574488]

Rosenberry TL. Quantitative simulation of endplate currents at neuromuscular junctions of acetylcholine with acetylcholine receptor and acetylcholinesterase. Biophys J. 1979; 26:263–290. [PubMed: 262418]

Rossi SG, Rotundo RL. Transient interactions between collagen-tailed acetylcholinesterase and sulfated proteoglycans prior to immobilization on the extracellular matrix. J Biol Chem. 1996; 271:1979–1987. [PubMed: 8567647]

Rotundo, RL.; Fambrough, DM. Function and molecular structure of acetylcholinesterase. In: Engel, AG.; Franzini-Armstrong, C., editors. Myology. McGraw-Hill; New York: 1994. p. 607-623.

Rotundo RL, Rossi SG, Anglister L. Transplantation of quail collagen-tailed acetylcholinesterase molecules onto the frog neuromuscular synapse. J Cell Biol. 1997; 136:367–374. [PubMed: 9015307]

Rotundo RL, Rossi SG, Kimbell LM, Ruiz C, Marrero E. Targeting acetylcholinesterase to the neuromuscular synapse. Chem Biol Interact. 157–158:15–21.

Roy A, Kucukural A, Zhang Y. I-TASSER: a unified platform for automated protein structure and function prediction. Nat Protoc. 2010; 5:725–738. [PubMed: 20360767]

Roy A, Yang J, Zhang Y. COFACTOR: an accurate comparative algorithm for structure-based protein function annotation. Nucleic Acids Res. 2012; 40:W471–W477. [PubMed: 22570420]

Schwede T, Kopp J, Guex N, Peitsch MC. SWISS-MODEL: an automated protein homology-modeling server. Nucleic Acids Res. 2003; 31:3381–3385. [PubMed: 12824332]

Sigoillot SM, Bourgeois F, Lambergeon M, Strochlic L, Legay C. ColQ controls postsynaptic differentiation at the neuromuscular junction. J Neurosci. 2010; 30:13–23. [PubMed: 20053883]

Sikorav JL, Duval N, Anselmet A, Bon S, Krejci E, Legay C, Osterlund M, Reimund B, Massoulié J. Complex alternative splicing of acetylcholinesterase transcripts in Torpedo electric organ; primary structure of the precursor of the glycolipid-anchored dimeric form. EMBO J. 1988; 10:2983–2993. [PubMed: 3181125]

Simon S, Krejci E, Massoulie J. A four-to-one association between peptide motifs: four C terminal domains from cholinesterase assemble with one proline-rich attachment domain (PRAD) in the secretory pathway. EMBO J. 1998; 17:6178–6187. [PubMed: 9799227]

Spivak M, Bereman MS, Maccoss MJ, Noble WS. Learning score function parameters for improved spectrum identification in tandem mass spectrometry experiments. J Proteome Res. 2012; 11(9): 4499–4508. [PubMed: 22866926]

Strochlic L, Cartaud A, Labas V, Hoch W, Rossier J, Cartaud J. MAGI-1c: a synaptic MAGUK interacting with MuSK at the vertebrate neuromuscular junction. J Cell Biol. 2001; 153:1127–1132. [PubMed: 11381096]

Vigny M, Bon S, Massoulié J, Leterrier F. Active-site catalytic efficiency of acetylcholinesterase molecular forms in Electrophorus, Torpedo, rat, and chicken. Eur J Biochem. 1978; 85:317–323. [PubMed: 648523]

Vigny M, Martin G, Grotendorst GR. Interactions of asymmetric forms of acetylcholinesterase with basement membrane components. J Biol Chem. 1983; 258:8794–8798. [PubMed: 6863310]

Wessel D, Flugge UI. A method for the quantitative recovery of protein in dilute solution in the presence of detergents and lipids. Anal Biochem. 1984; 138:141–143. [PubMed: 6731838]

Yang WD, Gomes RR Jr, Alicknavitch M, Farach-Carson MC, Carson DD. Perlecan domain I promotes fibroblast growth factor 2 delivery in collagen I fibril scaffolds. Tissue Eng. 2005; 11:76. [PubMed: 15738663]

Younkin SG, Rosenstein C, Collins PL, Rosenberry TL. Cellular localization of the molecular forms of acetylcholinesterase in rat diaphragm. J Biol Chem. 1982; 257:13630–13637. [PubMed: 7142169]

Zhang Y. I-TASSER server for protein 3D structure prediction. BMC Bioinformatics. 2008; 9:40.10.1186/1471-2105-9-40 [PubMed: 18215316]

Zhang Y, Skolnick J. Scoring function for automated assessment of protein structure template quality. Proteins. 2004; 57:702–710. [PubMed: 15476259]

Zhang Y, Skolnick J. TM-align: a protein structure alignment algorithm based on the TM-score. Nucleic Acids Res. 2005; 33:2302–2309. [PubMed: 15849316]

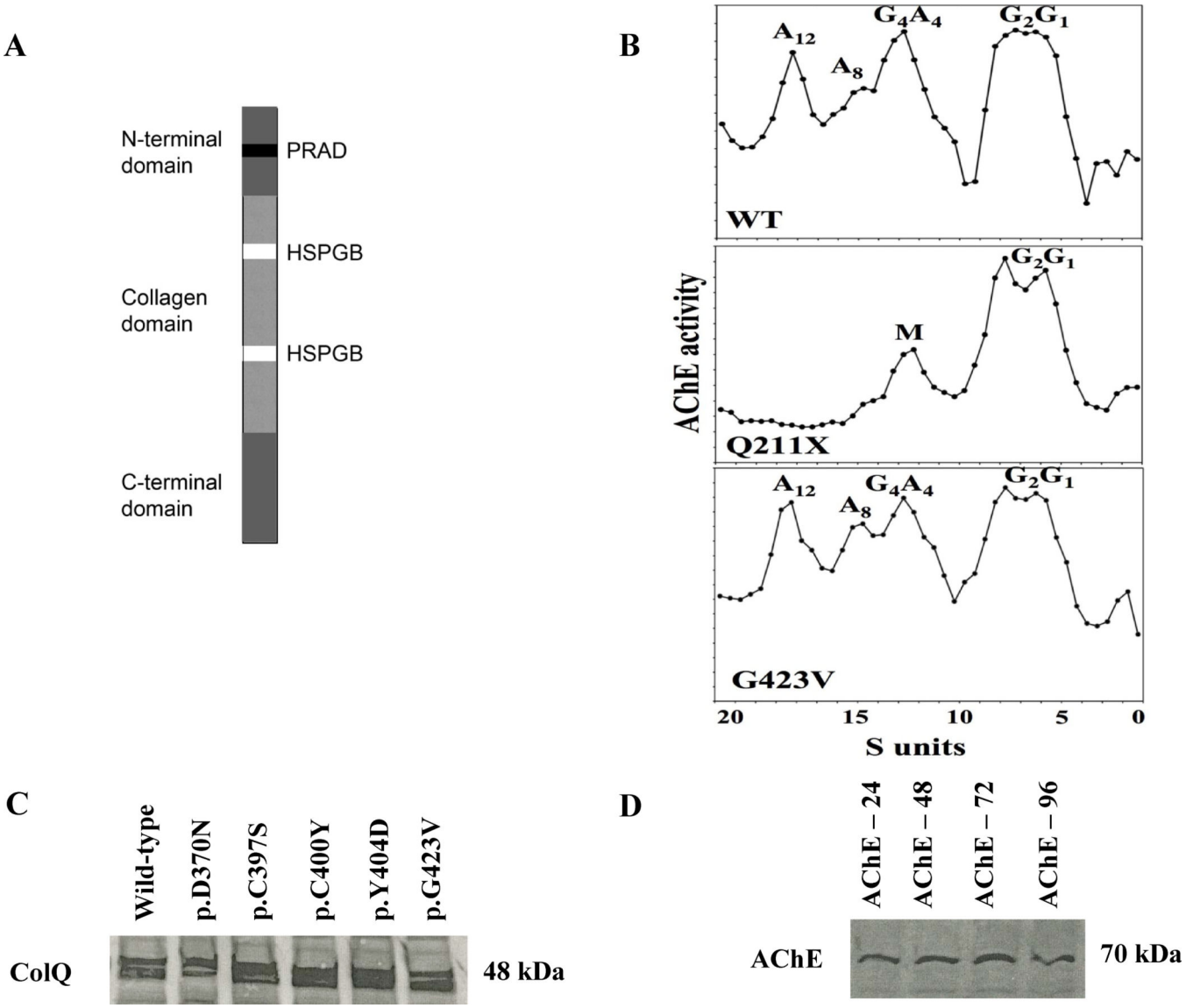

Fig. 1.

The COOH-terminal ColQ mutations do not impair assembly of AChE with ColQ. **(a)** Schematic diagram showing the central triple-helical collagen domain is surrounded by non-collagenous NH2-terminal and COOH-terminal domains of ColQ. The PRAD region is within the NH2-terminal domain and the two HSPG-binding (HSPGB) motifs are located in the collagen domain. **(b)** Representative sucrose density gradients. Truncation mutations such as p. Gln211* result only in the globular forms of the enzyme (G_1 and G_2) plus an M peak. COOH-terminal mutations such as p.Gly423Val do not alter the assembly of ColQ with $AChE_T$ and the sedimentation profile is similar to that of WT. The amplitudes of the A_{12} and the G_1 and G_2 peaks are highly variable from preparation to preparation. **(c)** Overexpression of ColQ protein on COS-7 cells transfected with WT ColQ and mutant constructs. Crude cell lysates were immunoblotted with ColQ antibody. **(d)** Crude cell lysates of AChE overexpressed protein on COS-7 cells were immunoblotted with AChE

antibody. Western blot variations of transfection efficiency were corrected by monitoring the expression of β-actin in the immunoblots, data not shown.

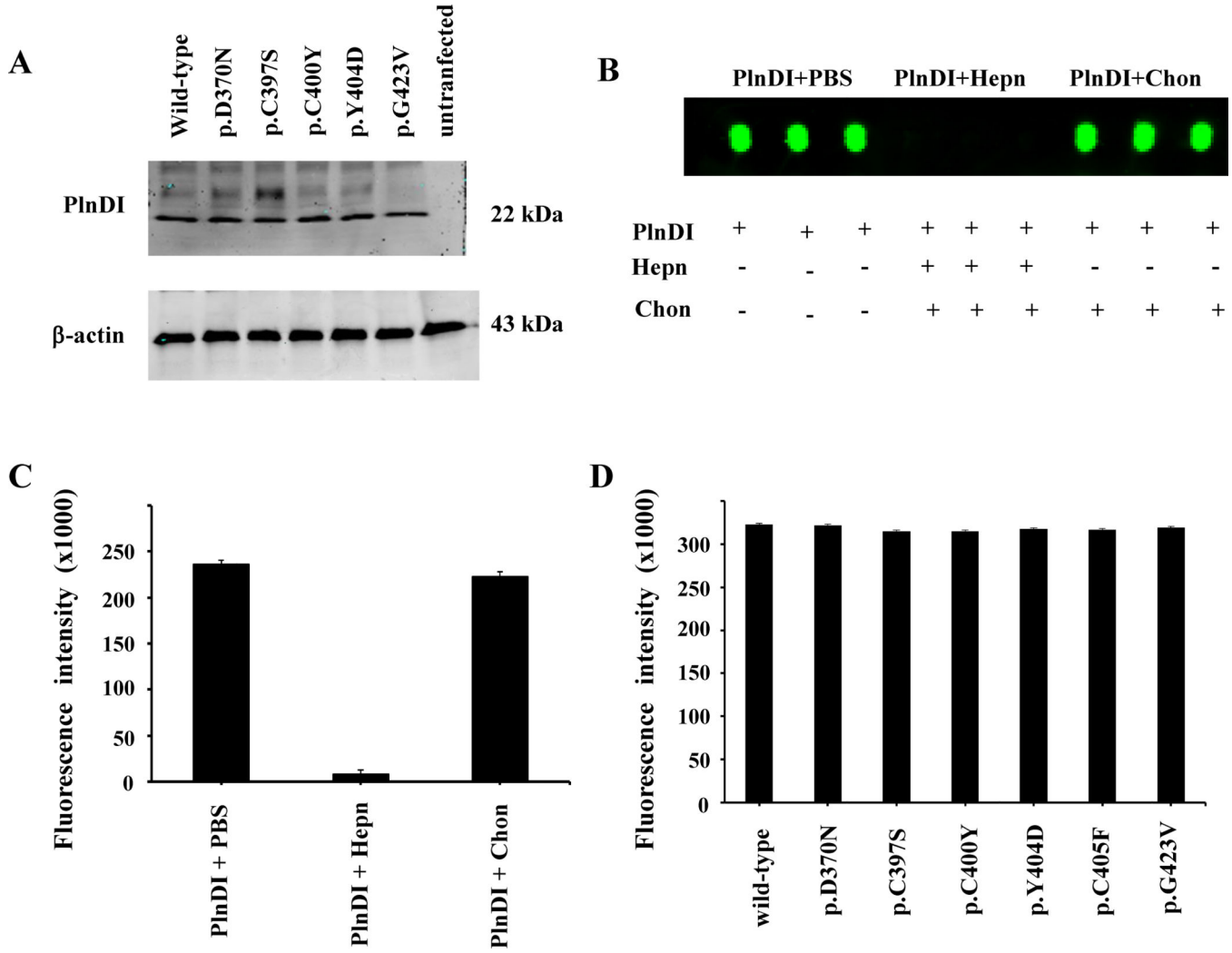

Fig. 2.

The COOH-terminal ColQ mutations do not impair binding of ColQ subunit to perlecan. **(a)** Co-immunoprecipitation experiments were performed after co-expression of $AChE_T$ and WT ColQ or mutants in inducible HEK-EBNA cells expressing PlnDI. The protein complex between ColQ and perlecan proteins was co-immunoprecipitated with goat antibody against ColQ. The immunoprecipitates were digested with heparitinases (50 IU/g protein) and chondroitinase (1 U/mg protein), and analyzed by Western blots using rabbit antibody against perlecan. The housekeeping β-actin protein was used to normalize the protein expression. Only the control lane, non-transfected HEK-EBNA cells, showed no PlnDI band, ~22 kDa. Endogenous perlecan will not appear in the blots due to its enormous size and glycosaminoglycan chains. **(b)** Dot-blot analyses of ColQ interaction with PlnDI. The PlnDI was immobilized on nitrocellulose in its native form or after digestion with heparinases I, II, and III (Hepn) or chondroitinase AC (Chon). A_{12} form binding was determined by ColQ antibody, the samples were blotted in triplicate on nitrocellulose membrane. **(c)** Bar graph summarizes fluorescence measurements performed on dot blot. **(d)** Summary of the dot blots binding assays. The purified AChE A_{12} asymmetric forms for

each mutant were incubated on nitrocellulose membrane blotted with PlnDI. The bar graph summarizes measurements dot blot performed on each mutant.

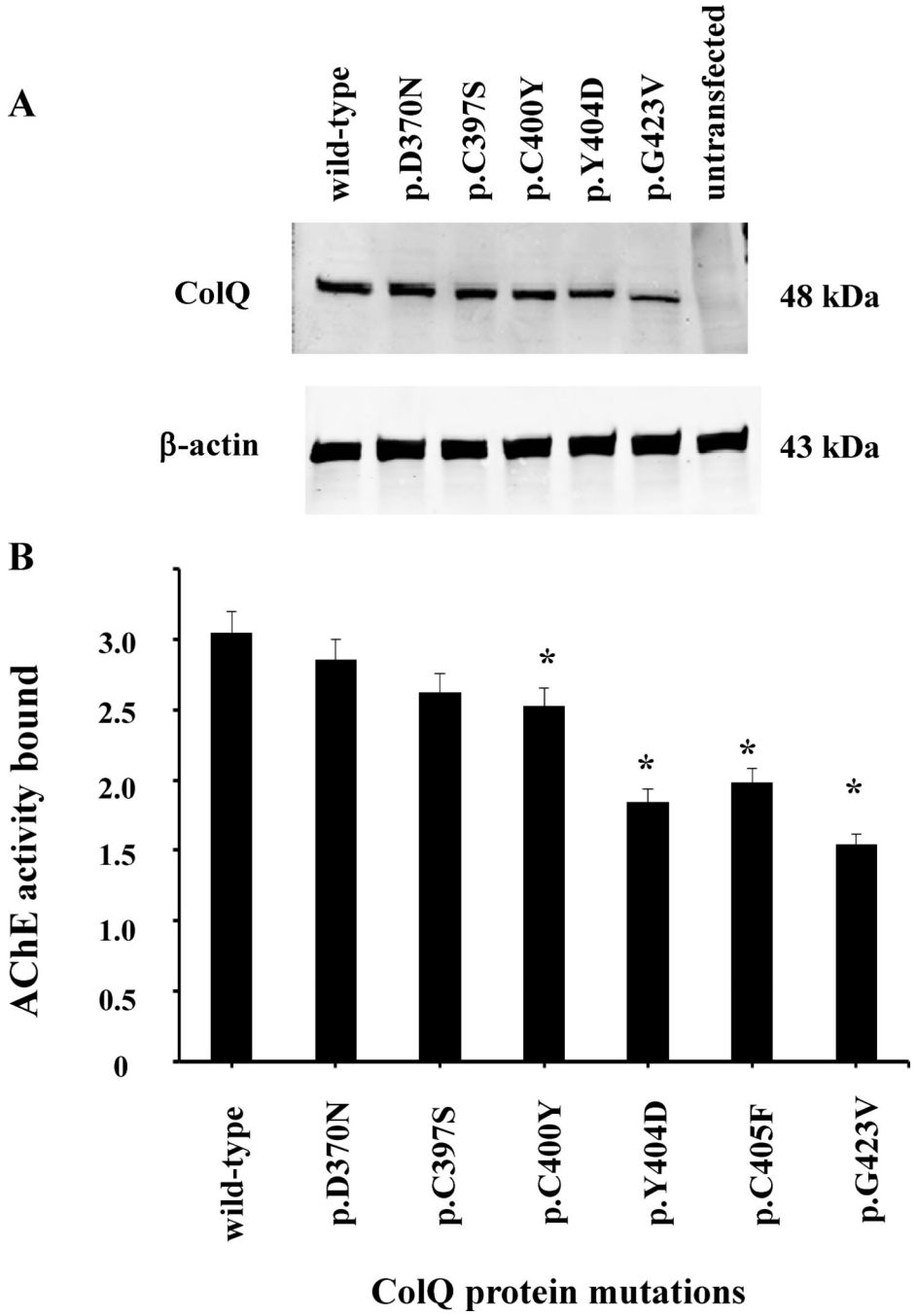

Fig. 3.

The COOH-terminal ColQ mutations impair the binding of the ColQ subunit to MuSK. **(a)** Co-immunoprecipitation experiments were performed after co-transfection of HEK-293 cells with either WT ColQ or one of the ColQ mutants, p.Asp370Asn, p.Cys397Ser, p.Cys400Tyr, p.Tyr404Asp, or Gly423Val, and with WT MuSK. The protein complex between MuSK and ColQ proteins was co-immunoprecipitated with rabbit MuSK antibody. The immunoprecipitates were analyzed by Western blots using goat antibody against ColQ. The WT ColQ protein (48 kDa) showed the strongest interaction with MuSK, while

p.Gly423Val showed the weakest interaction with MuSK. The control lane, un-transfected HEK cells, showed no ColQ band. The housekeeping β-actin protein was used as a control to verify that all the samples had the same amount of loaded protein. **(b)** The binding assays, where the 96-well plate was coated with pure MuSK. The purified AChE A_{12} asymmetric forms were overlaid on the plate. The AChE enzymatic activity was used to measure the binding of AChE A_{12} asymmetric forms to MuSK. Only results for the mutants p.Cys400Tyr, p.Tyr404Asp, p.Cys405Phe and p.Gly423Val had statistical significance (*$P < 0.05$).

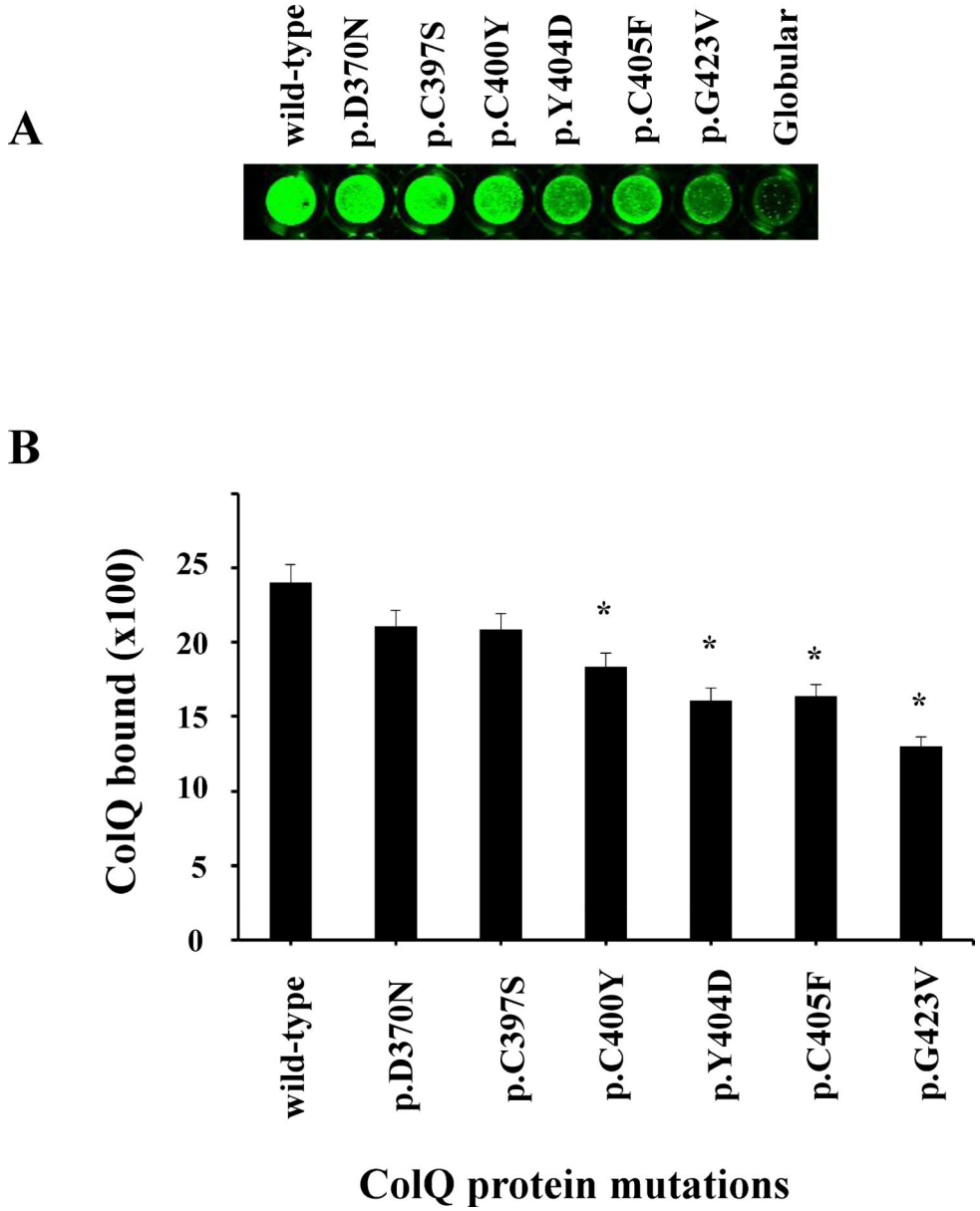

Fig. 4.

The COOH-terminal ColQ mutations impair binding of ColQ subunit to the basal lamina. **(a)** The binding assays, where the 96-well plate was coated with BME. The purified AChE A_{12} asymmetric forms from each mutant and wild type were overlaid on top of BME. The binding affinity of ColQ was measured by In-Cell Western, where the ColQ binding was measured by the fluorescence intensity. In comparison with the WT, all mutants showed different levels of fluorescence intensity. The globular AChE forms were used as a negative control**. (b)** The quantitative analysis shown in the graph demonstrates that the WT had the highest fluorescent signal intensity; mutants p.Asp370Asn, and p.Cys397Ser did not have statistical significance, and p.Cys400Tyr, p.Tyr404Asp, p.Cys405Phe and p.Gly423Val had the lowest fluorescent intensity, all statistically significant (*$P < 0.05$).

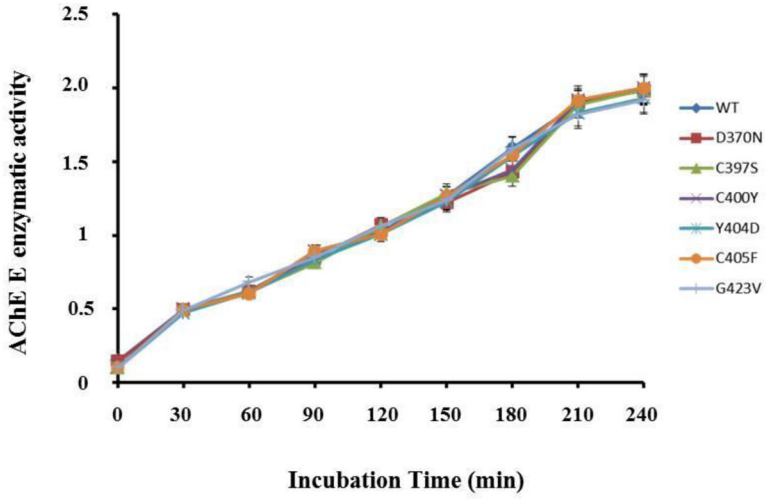

Fig. 5.

The COOH-terminal ColQ mutations do not affect AChE enzymatic activity. Purified A_{12} asymmetric forms were used to quantify the AChE enzymatic activity in solution. The WT and p.Asp370Asn, p.Cys397Ser, p.Cys400Tyr, p.Tyr404Asp, p.Cys405Phe, and p.Gly423Val mutants purified A_{12} forms' AChE activity was quantified by Ellman assay. The results confirmed that COOH-terminal ColQ mutations did not affect the enzyme efficiency. The graph showed a linear trend over time. The data showed that AChE tetramers attached to all ColQ mutants had the same AChE esterase activity as the WT ColQ subunit attached to the AChE catalytic subunit.

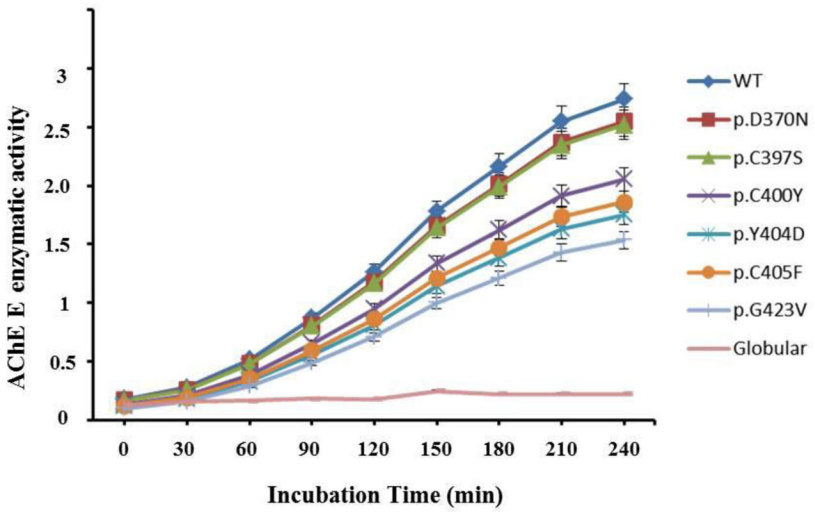

Fig. 6.

The COOH-terminal ColQ mutations impair binding of asymmetric AChE forms to BME. The purified A_{12} AChE asymmetric forms were incubated with BME. Then, the AChE esterase enzymatic activity was measured at different time points as shown in the graph by performing the Ellman assay. The data showed that mutants' p.Asp370Asn and p.Cys397Ser had slightly lower levels of AChE esterase activity than WT. The mutants p.Cys400Tyr, p.Tyr404Asp, and p.Cys405Phe had lower enzymatic activity than WT, and the p.Gly423Val showed the lowest level of AChE enzymatic activity; all were statistically significant (*$P < 0.05$). The globular AChE forms were used as a negative control.

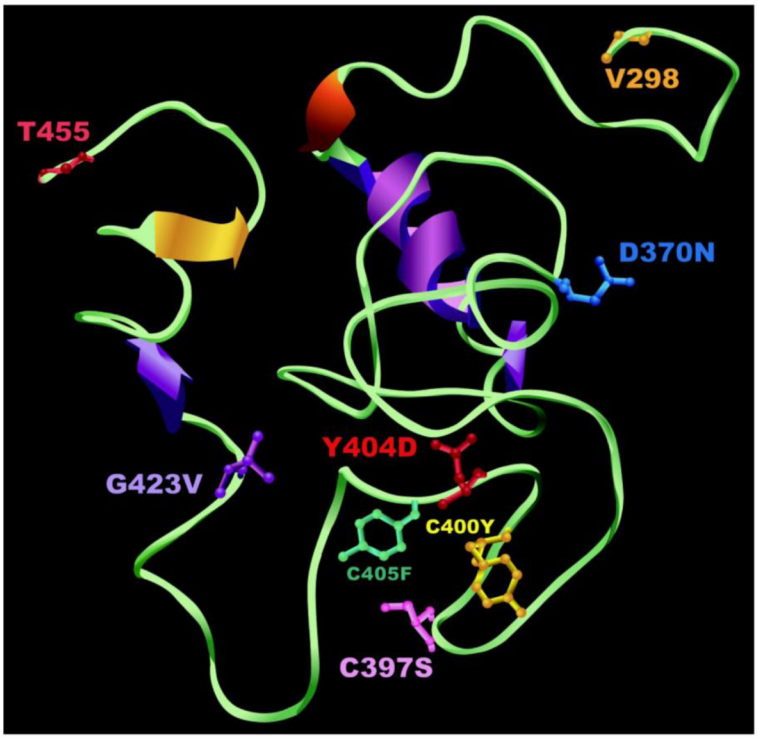

Fig. 7.

Theoretical tertiary structure of COOH-terminal ColQ subunit (single strand showing only). The 3D structure is represented in ribbon diagram; the α-helices are in magenta, β-sheets in yellow, and coil in green. The mutated residue side chains are illustrated as follows: p.D370N in blue, p.Cys397Ser in pink, p.Cys400Tyr in yellow, p.Tyr404Asp in red, p.Cys405Phe in green, and p.Gly423Val in purple. All the mutated residues occurred in the coil secondary structure. The initial residue of the COOH-terminal domain is V298 in orange, and the last residue is T455 in red. Reference Protein Sequence: NP_005668.2.

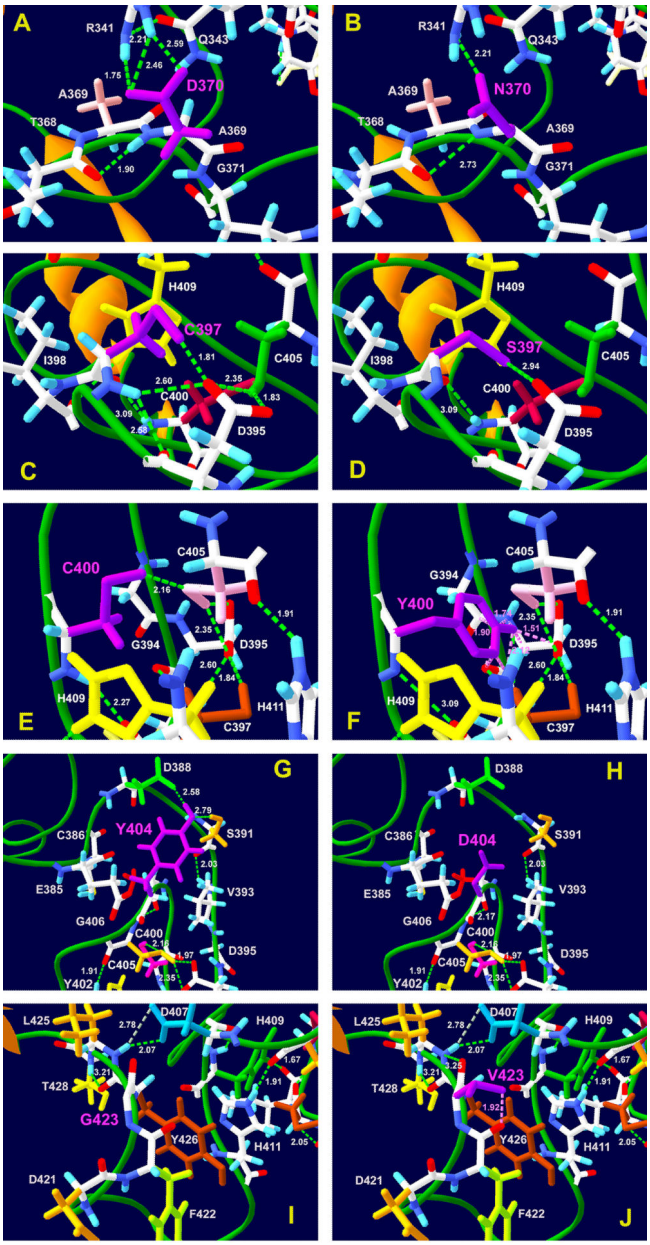

Fig. 8.

ColQ mutations affecting hydrogen-bonding interactions. Three-dimensional structure of the ColQ COOH-terminal domain is represented in a ribbon diagram, where α-helices are in orange, coils are in green, and hydrogen bonds (H-bonds) are shown with green dotted lines. Hydrogen atoms are in sky blue, oxygen atoms in red, and peptide bonds in dark blue. **(a)** The negatively charged side chain of aspartic acid (D) 370, a polar residue (magenta), interacts with the positively charged side chain of arginine (R) 341, a polar charged residue creating three H-bonds with 2.59, 2.46, and 1.75 Å distances, and a fourth backbone-backbone H-bond of 1.90 Å is between the amine group of D370 and the carboxyl group of T368, a polar hydroxyl residue. Polar charged R341 forms a fifth H-bond of 2.21 with amide polar residue Q343. **(b)** The p.Asp370Asn mutation changes the aspartic acid negatively

charged side chain to an asparagine amide side chain. The new polar N370 residue loses three H-bonds with 2.46, 1.75, and 2.21 Å, but increases the distance of H-bonds from 1.90 to 2.73, and reduces 2.59 to 2.21 Å. **(c)** The sulfur-containing side chain of cysteine (C) 397, a hydrophobic residue (magenta), forms an H-bond of 1.81 Å with aspartic acid (D) 395 acidic side chain, and there is an amide (blue) interaction between C397 and polar D395 residue creating a side chain-backbone H-bond of 2.60 Å, and a backbond interaction between C397 and D395 residue to form the third H-bond (2.58 Å). A fourth backbone H-bond is between C397 and sulfur side chain C400 (red) residue, 3.09 Å. Two more H-bonds are created between D395 and another cysteine, C405 (green), with 2.35 and 1.83 Å. **(d)** The p.Cys397Ser mutation changes from the cysteine sulfur-containing side chain to the hydroxyl side chain serine, a polar residue. S397 (magenta) residue loses the 2.60, 2.58, 2.35, and 1.83 Å H-bonds, but creates a change by increasing the H-bond between S397 and D395 from 1.81 to 2.94 Å. **(e)** The side chain of C400 hydrophobic residue (magenta) has two H-bonds, one with backbone of cysteine C397 (orange) residue (2.27 Å), the second with a polar side chain of C405 (pink) (2.16 Å) to form a disulfide bond; four more H-bonds are formed between C405 and D395 (2.35 Å), C405 and H411 (1.91 Å), H409 and D395 (2.60 Å), and C397 and D395 (1.84 Å). **(f)** This mutation changes from cysteine, a smaller residue, to a larger aromatic side chain tyrosine (magenta) residue, where Y400 polar residue loses one 2.16 Å H-bond. However, its phenolic *COLQ mutants causing DEA* ringside chain gains four new H-bonds, two with D395 backbone (1.51 and 1.90 Å), and another two with C397 (2.12 Å) and G394 (1.74 Å). **(g)** The tyrosine (Y) 404 phenolic group (magenta) side chain creates two H-bonds: one with the polar side chain of S391 (orange) (2.79 Å), and the other with the D388 (green) negatively charged side chain (2.58 Å). Other H-bonds are also formed between C405 and C400 (2.16 Å), S391 and V393 (2.03 Å), and C405 and Y402 (1.91 Å), and two between C405 and D395 (2.35 and 1.97 Å). **(h)** The Y404 (magenta) mutation change to a smaller acidic residue produces the loss of 2.79 and 2.58 Å H-bonds between Y404 and S391 and D388 residues. **(i)** A hydrophobic G423 residue does not form any H-bonds with any surrounding amino acids because it lacks a side chain. However, the surrounding residues create the following H-bonds: L425-D407 (2.78 Å); L425-D407 (2.07 Å) and T428-Y426 (3.21 Å). **(j)** The aliphatic side chain of hydrophobic V423 residue creates two new H-bonds: one with the aromatic side chain of the polar F422 residue (1.92 Å), and the second (3.25 Å) between the backbones of V423 and the L425 aliphatic residues.

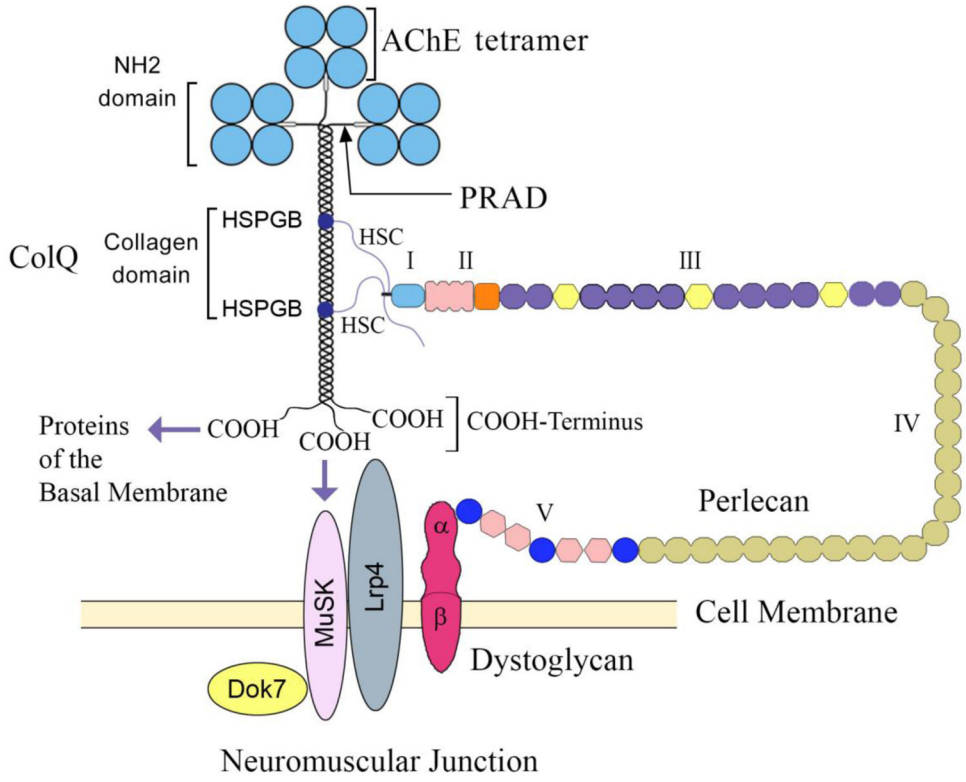

Fig. 9.

Diagram showing the most important molecular interactions of human ColQ. The diagram shows the assembly of each ColQ triple-helix with globular AChE homotetramers through its proline-rich attachment domain (PRAD) located at the NH_2 terminus. Two heparan sulfate proteoglycan binding (HSPGB) sites located at the collagen domain of ColQ bind to two heparan sulfate polysaccharide chains (HSC), or glycosaminoglycans that are covalently attached to the NH_2 terminus (domain I) of perlecan. The COOH terminus (domain V) of perlecan in turn binds to α-dystroglycan. Finally, the COOH terminus of ColQ binds to MuSK, but also—based on our results—to other proteins of the basal membrane.

Table 1

Protein identification by sensitive-tandem mass spectrometry

Basal Membrane Extract Identified Proteins[b]	Gene Name	Molecular Weight	Quantitative Value, %[c]
Laminin subunit α1[d]	Lama1	338 kDa	1
Laminin subunit γ1	Lamc1	177 kDa	0.68
Nidogen-1	Nid1	137 kDa	0.55
Laminin subunit β1	Lamb1	202 kDa	0.51
Perlecan (heparan sulfate proteoglycan 2)	Hspg2	470 kDa	0.21
Laminin subunit γ1	Lamc1	87 kDa	0.10
Collagen, type IV, α2	Col4a2	162 kDa	0.09
Myosin-9	Myh9	226 kDa	0.06
Vimentin	Vim	52 kDa	0.05
Nidogen-2	Nid2	154 kDa	0.05
Fibrinogen beta chain	Fgb	55 kDa	0.04
Basement membrane-specific heparan sulfate proteoglycan core protein Hspg2	Hspg2	398 kDa	0.04
Plasminogen	Plaur	91 kDa	0.04
Fibrinogen gamma chain	Fgg	49 kDa	0.03
Fibronectin 1	Fn1	240 kDa	0.03
Fibulin 1	Fbln1	78 kDa	0.03
Peroxidasin homolog (Drosophila)	Pxdn	165 kDa	0.02

[a] LC-MS/MS analysis was performed with a Thermo Scientific LTQ linear ion trap mass spectrometer in conjunction with a Paradigm MG4 HPLC. The basement membrane extract was derived from murine Engelbreth-Holm-Swarm (EHS) sarcoma cells.

[b] Identified proteins in the BME, derived from murine Engelbreth-Holm-Swarm tumor, by mass spectrometry, where laminin, nidogen, perlecan, and collagen IV were the most abundant.

[c] The quantitative value represents the abundance of the protein compared to the most abundant protein.

[d] Laminin alpha-1 was the most abundant protein.

Table 2

Hydrogen bond interaction changes due to COOH-terminal ColQ mutations[a]

Mutation	H-Bonds (Å) before mutation[b]	H-Bonds (Å) lost after mutation[c]	H-Bonds (Å) change after mutation[d]	H-Bonds (Å) gain after mutation[e]
D370N	D370-R341 (2.59)	D370-R341 (2.46)	N370-R341	
	D370-R341 (2.46)	D370-R341 (1.75)	2.59 →2.21	
	D370-R341 (1.75)	R341-Q343 (2.21)	N370-T368	
	R341-Q343 (2.21)		1.90→2.73	
	D370-T368 (1.90)			
C397S	C397-D395 (1.81)	C397-D395 (2.60)	S397-D395	
	C397-D395 (2.60)	C397-R341 (2.58)	1.81→ 2.94	
	C397-D395 (2.58)	D395-C405 (2.35)		
	C397-C400 (3.09)	D395-C405 (1.83)		
	D395-C405 (2.35)			
	D395-C405 (1.83)			
C400Y	C400-C405 (2.16)	C400-C405 (2.16)	C400-C397 (2.27)	Y400-D395 (1.51)
	C400-C397 (2.27)		2.27 → 3.09	Y400-D395 (1.90)
	C405-C397 (2.35)			Y400-C397 (2.12)
	C405-H411 (1.91)			Y400-G394 (1.74)
	H409-D395 (2.60)			
	C397-D395 (1.84)			
Y404D	Y404-S391 (2.79)	Y404-S391 (2.79)		
	Y404-D388 (2.58)	Y404-D388 (2.58)		
	C405-Y402 (1.91)			
	S391-V393 (2.03)			
	C405-C400 (2.16)			
	C405-D395 (1.97)			
	C405-D395 (2.35)			
G423V	L425-D407 (2.78)			V423-L425 (3.25)
	L425-D407 (2.07)			V423-F422 (1.92)
	T428-Y426 (3.21)			
C405F	C405-C400 (2.16)	C405-C400 (2.16)		F405-C397 (3.97)
	G405-D395 (1.83)	G405-D395 (1.83)		F405-C397 (2.19)
	C405-D395 (2.35)	C405-D395 (2.35)		F405-H411 (1.82)

[a] Because the residue mutations usually affect the conformation of the residues in the neighborhood, the table lists the H-bonds before and after the residue mutations based on the modeled structure.

[b] The interacting amino acids and the hydrogen bonds distances found before the mutation.

[c] The number of hydrogen bonds lost after introducing the mutation.

[d] The hydrogen bond changes induced by the mutation.

[e] New hydrogen bonds created by the mutation.